

12

AFGL-TR-85-0097

**ESTIMATION OF SCALAR MOMENTS FROM
EXPLOSION-GENERATED SURFACE WAVES**

J. L. Stevens

**S-CUBED
P. O. Box 1620
La Jolla, California 92038-1620**

Scientific Report No. 2

April 1985

**Approved for Public Release,
Distribution Unlimited**

DTIC
ELECTE
OCT 16 1985
S **D**
B

**AIR FORCE GEOPHYSICS LABORATORY
Air Force Systems Command
United States Air Force
Hanscom Air Force Base
Massachusetts 01731**

85 10 16 131

MSF

AD-A160 327

DTIC FILE COPY

Sponsored by

Defense Advanced Research Projects Agency (DOD)
Defense Sciences Office, Geophysical Sciences Division
DARPA/DSO Explosion Source and Yield Estimation Research
ARPA Order No. 5308

Issued by the Air Force Geophysics Laboratory
Under Contract F19628-85-C-0045

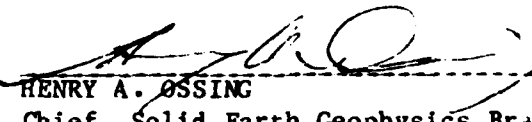
The views and conclusions contained in this document are those of the author(s) and should not be interpreted as representing the official policies, either expressed or implied, of the Defense Advanced Research Projects Agency or the United States Government.

W/O 11287

This technical report has been reviewed and is approved for publication.

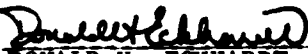


ROBERT A. GRAY
Contract Manager



HENRY A. OSSING
Chief, Solid Earth Geophysics Branch

FOR THE COMMANDER



DONALD H. ECKHARDT
Director
Earth Sciences Division

This report has been reviewed by the ESD Public Affairs Office (PA) and is releasable to the National Technical Information Service (NTIS).

Qualified requestors may obtain additional copies from the Defense Technical Information Center. All others should apply to the National Technical Information Service.

If your address has changed, or if you wish to be removed from the mailing list, or if the addressee is no longer employed by your organization, please notify AFGL/DAA, Hanscom AFB, MA 01731. This will assist us in maintaining a current mailing list.

UNCLASSIFIED

SECURITY CLASSIFICATION OF THIS PAGE

AD-A160327

REPORT DOCUMENTATION PAGE

1a. REPORT SECURITY CLASSIFICATION Unclassified		1b. RESTRICTIVE MARKINGS	
2a. SECURITY CLASSIFICATION AUTHORITY		3. DISTRIBUTION/AVAILABILITY OF REPORT Approved for public release, distribution unlimited.	
2b. DECLASSIFICATION/DOWNGRADING SCHEDULE			
4. PERFORMING ORGANIZATION REPORT NUMBER(S) SSS-R-85-7232		5. MONITORING ORGANIZATION REPORT NUMBER(S) AFGL-TR-85-0097	
6a. NAME OF PERFORMING ORGANIZATION S-CUBED	6b. OFFICE SYMBOL (If applicable)	7a. NAME OF MONITORING ORGANIZATION Air Force Geophysics Laboratory (LWH)	
6c. ADDRESS (City, State and ZIP Code) P. O. Box 1620 La Jolla, California 92038-1620		7b. ADDRESS (City, State and ZIP Code) Hanscom Air Force Base Massachusetts 01731	
8a. NAME OF FUNDING/SPONSORING ORGANIZATION	8b. OFFICE SYMBOL (If applicable)	9. PROCUREMENT INSTRUMENT IDENTIFICATION NUMBER F19628-85-C-0045	
8c. ADDRESS (City, State and ZIP Code)		10. SOURCE OF FUNDING NOS.	
		PROGRAM ELEMENT NO. 62714E	PROJECT NO. 5A10
		TASK NO. DA	WORK UNIT NO. AW
11. TITLE (Include Security Classification) ESTIMATION OF SCALAR MOMENTS FROM EXPLOSION-GENERATED SURFACE WAVES			
12. PERSONAL AUTHOR(S) J. L. Stevens			
13a. TYPE OF REPORT Scientific Rpt No. 2	13b. TIME COVERED FROM _____ TO _____	14. DATE OF REPORT (Yr., Mo., Day) 1985 April	15. PAGE COUNT 74
16. SUPPLEMENTARY NOTATION Sponsored by Defense Advanced Research Projects Agency (DOD), Defense Sciences Office, Geophysical Sciences Division, DARPA/DSO Explosion Source and Yield Estimation Research, ARPA Order No. 5308 <i>cont. 4 pgs</i>			
17. COSATI CODES		18. SUBJECT TERMS (Continue on reverse if necessary and identify by block number)	
FIELD	GROUP	SUB. GR.	
			Explosion Seismology; Rayleigh Waves; Surface Waves; Explosion Yield Estimation.
19. ABSTRACT (Continue on reverse if necessary and identify by block number)			
<p>→ Rayleigh waves from underground nuclear explosions are used to estimate scalar moments for 40 Nevada Test Site (NTS) explosions and 18 explosions at the Soviet East Kazakh test site. The Rayleigh wave spectrum is written as a product of functions that depend on the elastic structure of the travel path, the elastic structure of the source region and the Q structure of the path. We use our results to examine the worldwide variability of each factor and the resulting variability of surface wave amplitudes. The path elastic structure and Q structure are found by inversion of Rayleigh wave phase and group velocities and spectral amplitudes. The Green's function derived from this structure is used to estimate the moments of explosions observed along the same path.</p> <p>This procedure produces more consistent amplitude estimates than conventional magnitude measurements. Network scatter in log moment is typically 0.1. (over)</p>			
20. DISTRIBUTION/AVAILABILITY OF ABSTRACT UNCLASSIFIED/UNLIMITED <input type="checkbox"/> SAME AS RPT. <input checked="" type="checkbox"/> DTIC USERS <input type="checkbox"/>		21. ABSTRACT SECURITY CLASSIFICATION Unclassified	
22a. NAME OF RESPONSIBLE INDIVIDUAL Robert A. Gray		22b. TELEPHONE NUMBER (Include Area Code) (617) 861-3028	22c. OFFICE SYMBOL LWH

19-0117-17

UNCLASSIFIED

SECURITY CLASSIFICATION OF THIS PAGE

19. ABSTRACT (continued)

→ In contrast with time domain amplitudes, the elastic structure of the travel path causes little variability in spectral amplitudes. When the mantle Q is constrained to a value of approximately 100 at depths greater than 120 km, the inversion for Q and moment produces moments that remain constant with distance. Based on the best models available, surface waves from NTS explosions should be larger than surface waves from East Kazakh explosions with the same moment. Estimated scalar moments for the largest East Kazakh explosions since 1976 are smaller than the estimated moments for the largest NTS explosions for the same time period. This contrasts dramatically with m_b for the same events which show the opposite behavior.

Keywords:

topi

m_b
m sub b

UNCLASSIFIED

SECURITY CLASSIFICATION OF THIS PAGE

TABLE OF CONTENTS

<u>SECTION</u>	<u>PAGE</u>
I. INTRODUCTION	1
II. RAYLEIGH WAVES FROM AN EXPLOSION SOURCE	5
III. EXPLOSION DATA FOR THE NEVADA TEST SITE AND EAST KAZAKH	8
IV. DATA ANALYSIS AND INVERSION PROCEDURE	12
V. INVERSION FOR SHEAR VELOCITY STRUCTURE	21
VI. INVERSION FOR Q STRUCTURE AND SCALAR MOMENT	25
VII. SHEAR VELOCITY INVERSION RESULTS	29
VIII. Q CONSTRAINTS AND INVERSION RESULTS	32
IX. ESTIMATED MOMENTS FOR NTS AND EAST KAZAKH EXPLOSIONS	43
X. THE EFFECT OF SOURCE REGION STRUCTURE ON MOMENT ESTIMATES	50
XI. THE EFFECT OF MANTLE Q CONSTRAINTS ON MOMENT ESTIMATES	57
XII. SUMMARY AND CONCLUSIONS	63
XIII. REFERENCES	65

DTIC
ELECTE
 OCT 16 1985
B



Accession For	
NTIS GRA&I	<input checked="" type="checkbox"/>
DTIC TAB	<input type="checkbox"/>
Unannounced	<input type="checkbox"/>
Justification	
By _____	
Distribution/ _____	
Availability Codes	
Dist	Avail end/or Special
A-1	

LIST OF ILLUSTRATIONS

<u>FIGURE</u>		<u>PAGE</u>
1.	This figure illustrates the difficulty in measuring surface wave amplitudes using standard methods.....	2
2.	Path corrected amplitude and phase for the path NTS-GOL.....	4
3.	Surface wave paths from NTS to 24 WWSSN stations in the United States and Canada.....	9
4.	Surface wave paths from NTS to 12 SRO stations.....	10
5.	Surface wave paths from East Kazakh to 12 SRO stations.....	11
6.	Block diagram of surface wave analysis procedure...	13
7.	Six seismograms at WWSSN Station COL.....	15
8.	Six selected seismograms for Station COL.....	16
9.	Phase and group velocities for path from NTS to LON (1155 km).....	19
10.	Phase and group velocities for paths from NTS to WWSSN stations (top), NTS to SRO stations (middle) and East Kazakh to SRO stations (bottom).....	20
11.	Data misfit minima for NTS-AAM.....	23
12.	Initial and final shear velocity structures for path NTS-AAM.....	24
13.	Spectral amplitudes for NTS-LON path.....	26
14.	Shear velocity structures obtained by inversion for selected paths.....	30
15.	Path amplitude function S_2 for all paths from NTS and East Kazakh.....	31
16.	Source region structure used for the East Kazakh test site.....	33

LIST OF ILLUSTRATIONS (Continued)

<u>FIGURE</u>		<u>PAGE</u>
17.	Source region shear velocity models used for NTS and East Kazakh.....	37
18.	Excitation functions calculated at a depth of 1 km using the NTS structure and the East Kazakh structure.....	38
19.	Q structures found by Q/moment inversion for selected paths.....	40
20.	Attenuation coefficients for all paths from NTS and East Kazakh.....	41
21.	Estimated moments for the largest NTS and East Kazakh explosions since April 1976.....	48
22.	Excitation function S_1 calculated using the structures found for all paths from NTS and East Kazakh.....	51
23.	Excitation functions calculated using structures for all continental paths out of East Kazakh.....	52
24.	The dependence of the 20 second excitation function S_1 , ellipticity ϵ , phase velocity c , and group velocity U on the shallow shear velocity structure.....	54
25.	Excitation functions calculated from NTS and East Kazakh source region structures.....	55
26.	Station residuals with a mantle Q constraint of $\beta/Q = 40$	58
27.	Station residuals with mantle Q constraint of $\beta/Q = 25$	59
28.	Station residuals with a mantle Q constraint of $\beta/Q = 50$	60
29.	Station residuals with a mantle Q constraint of $\beta/Q = 100$	61

LIST OF TABLES

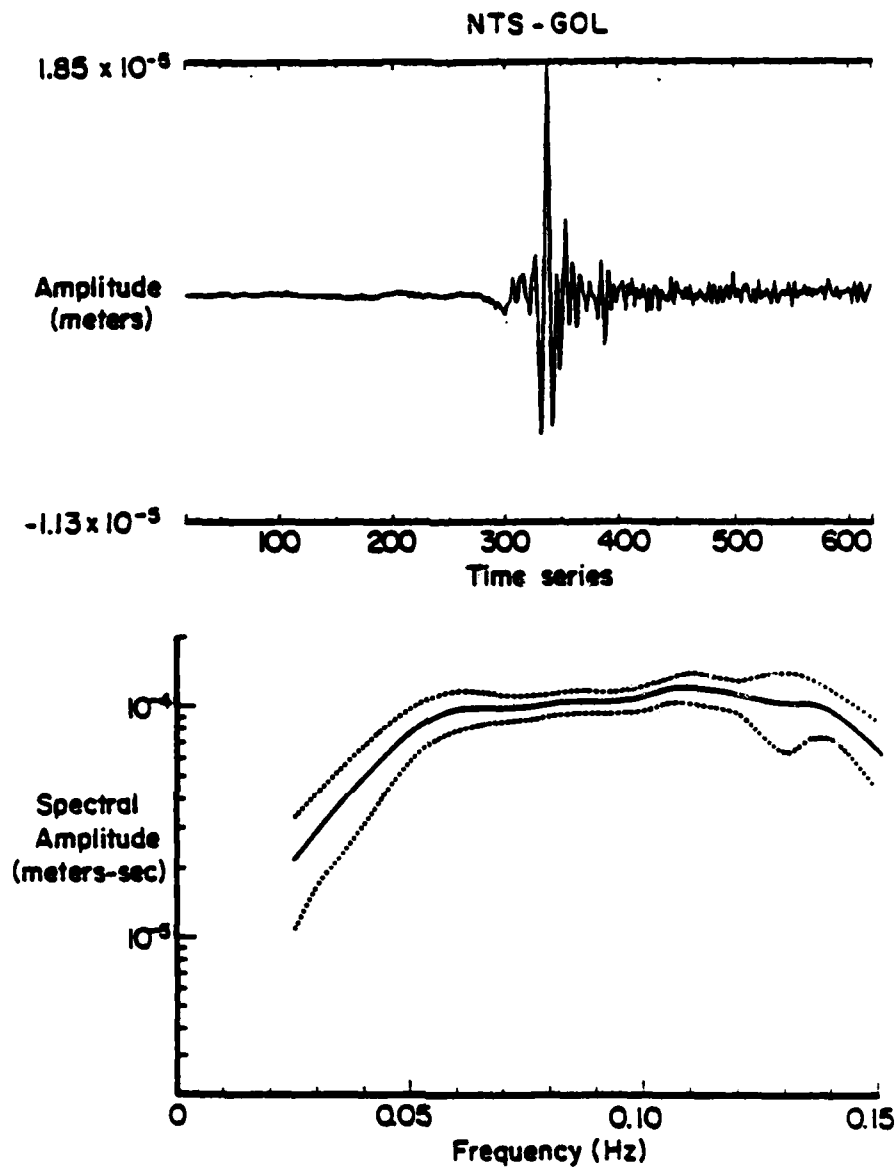
<u>TABLE</u>		<u>PAGE</u>
1	INITIAL PARAMETERS FOR TELVEL.....	17
2	NTS SOURCE REGION STRUCTURE.....	35
3	EAST KAZAKH SOURCE REGION STRUCTURE.....	36
4	AVERAGE 20 SECOND VALUES FOR NTS AND EAST KAZAKH PATHS (MKS UNITS).....	42
5	NTS EXPLOSIONS.....	44
6	EAST KAZAKH EXPLOSIONS.....	45
7	NTS SURFACE WAVE PATHS.....	46
8	EAST KAZAKH SURFACE WAVE PATHS.....	47

I. INTRODUCTION

Accurate and unbiased surface wave measurements are required if surface waves are to be used for treaty monitoring purposes. Conventional time domain M_S measurements provide a rough estimate of the size of the seismic source. Differences in travel path, however, cause variations in M_S that are unacceptable in cases where 0.1 magnitude unit may be important. On short paths (less than about 30 degrees), the seismogram is dominated by the Airy phase and 20 second amplitudes are difficult or impossible to measure accurately. On long paths, the surface waves are well-dispersed but attenuation differences can cause large amplitude variations. Since explosion yield estimation is usually done by defining a magnitude versus yield curve at one or more test sites, path differences and differences in station coverage can lead to a biased result when using this curve to estimate yields at an uncalibrated test site.

In this report, we describe a method for obtaining more stable and reliable surface wave measurements by using all of the information contained in the surface wave to estimate the Green's function for the path. We use Rayleigh waves from explosions at the Nevada Test Site (NTS) and the Soviet East Kazakh test site to find Green's functions for the paths between these test sites and SRO and WWSSN stations. The phase of the Green's function can be used to construct a phase-matched filter, which may be used to recover spectral amplitudes for surface waves from other events observed along nearby paths. The moment of the explosion can then be found by dividing the spectral amplitude by the amplitude of the Green's function for the path.

Figure 1 illustrates the difficulty in measuring surface wave amplitudes using standard methods. The top figure is a Rayleigh wave from an NTS explosion recorded at Station GOL, at a distance of 977 km. At this close distance many frequencies arrive at the same time, so that the seismogram is dominated by the Airy phase. A reliable 20

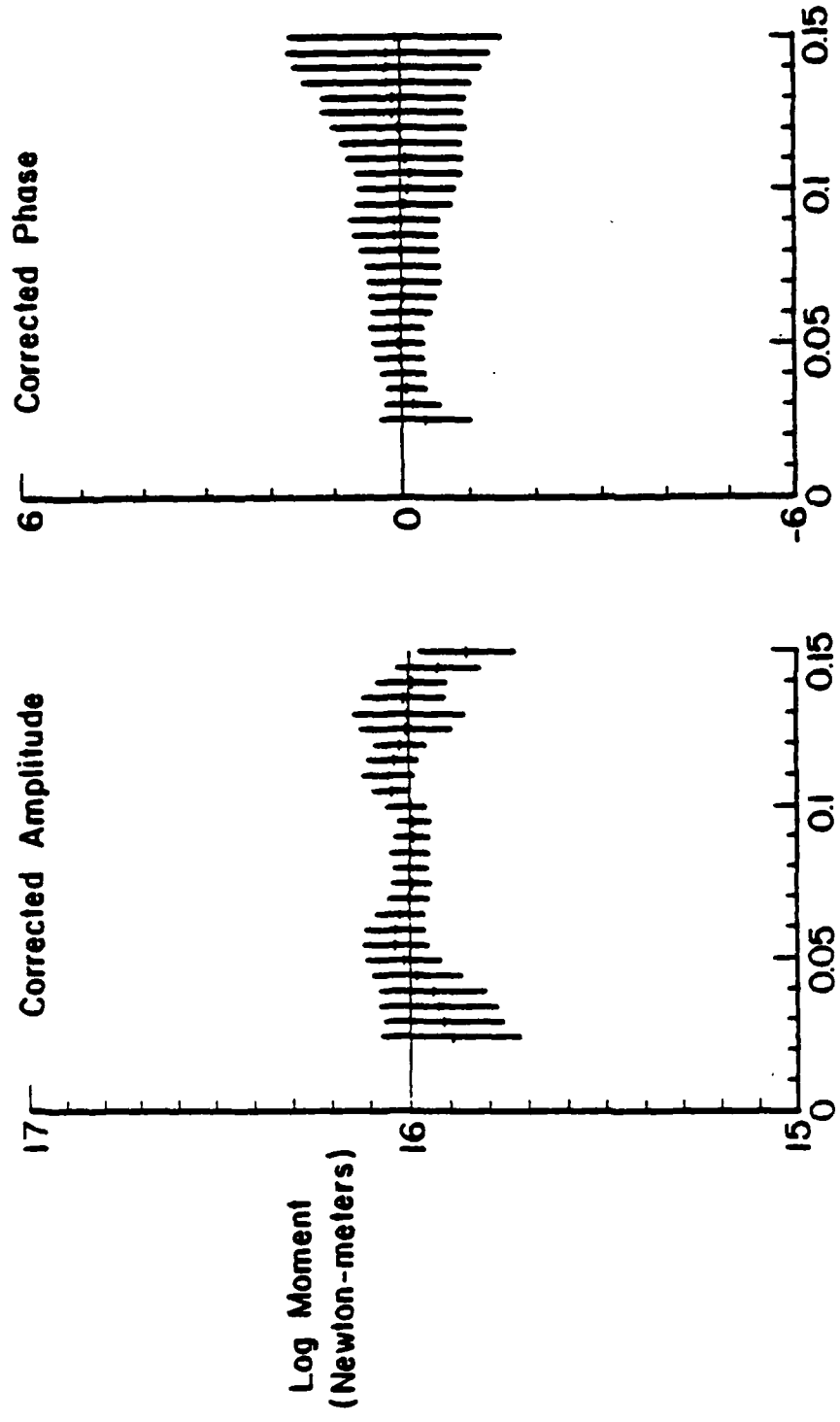


Seismogram and spectrum, NTS-GOL

Figure 1. This figure illustrates the difficulty in measuring surface wave amplitudes using standard methods. The top figure is a Rayleigh wave from the NTS explosion SANDREEF recorded at Station GOL. The seismogram is dominated by the Airy phase, so a reliable 20 second amplitude cannot be measured. The lower figure shows the average spectrum (solid line) and ± 1 standard deviation (dotted line) for 24 spectra at Station GOL. The amplitude depends strongly on the frequency measured.

second amplitude cannot be measured. Measuring the spectral amplitude instead of the seismogram removes this problem. The lower figure shows the average spectrum (solid line) and ± 1 standard deviation (dotted line) for 24 spectra at Station GOL. Another problem still remains, however. The amplitude depends strongly on the frequency measured, changing by a factor of 2 between 0.035 Hz and 0.05 Hz, and by a factor of 5 between 0.02 Hz and 0.05 Hz. Figure 2 shows the amplitude and phase of the spectrum after the path correction has been applied. Notice that in addition to correcting for path effects, the path correction is also a frequency correction, flattening the spectrum over the frequency band of interest.

The procedures recommended in this report are based on our experience applying surface wave analysis methods to real and synthetic data over the past few years. Bache, *et al.* (1978a) used inversion of surface wave dispersion to estimate the path structure between NTS and WWSSN Stations ALQ and TUC. Bache, *et al.* (1978b) used these structures to estimate the source size of NTS explosions. Rodi, *et al.* (1978) inverted Rayleigh waves from explosions at the French Sahara test site to estimate path structure in Africa. Our procedure is similar to that used by Bache, *et al.* (1978a), except that we use phase-matched filtering to recover phase velocities and spectral amplitudes; we invert for the Q structure of the path as well as the elastic structure; and the programs have been streamlined so many paths can be processed in an efficient manner. Tests of the phase-matched filtering and inversion programs are given by Wang, *et al.* (1981). The computer programs used in this study are described in detail in a report by Stevens, *et al.* (1982).



Path Correction Results - NTS to GOL

Figure 2. Path corrected amplitude and phase for the path NTS-GOL. The variation in amplitude with frequency is greatly reduced. The phase correction can be used to determine phase shifts (such as Rayleigh wave reversals) between events.

II. RAYLEIGH WAVES FROM AN EXPLOSION SOURCE

Our objective is to find the Green's function for a given source to receiver path which can be used to determine the explosion moment. Our approach to the problem has been to assume that the average path structure can be adequately modeled by a plane-layered, attenuating elastic medium. Since the explosions are located in a common source region, but the Rayleigh waves travel along different paths, we also use an approximation which allows us to separate the spectrum into source region and path dependent functions (Bache, *et al.*, 1978a). This approximation assumes energy conservation and no mode conversion when a Rayleigh wave crosses a boundary between adjacent plane-layered structures. The accuracy of this approximation has been demonstrated for selected cases by comparison with finite difference calculations by Glover and Harkrider (1981). We also assume an isotropic explosion source, neglecting nonisotropic source effects such as explosion-induced block motion and tectonic strain release. In the construction of the path Green's functions, we try to use events with little evidence of nonisotropic source effects.

Given these assumptions, we can write the vertical component of the Rayleigh wave as a product of functions each of which depends only on the source, the source region, or the path:

$$u(\omega, r) = M_0' S_1(\omega) S_2(\omega) \exp(-\gamma_2 r) / \sqrt{a_e \sin(r/a_e)} \exp\{i(\phi_0 - \omega r/c_2)\} \quad (1)$$

where M_0' is the normalized moment of the explosion discussed below, r is the source to receiver distance, a_e is the radius of the earth, c_2 is the frequency dependent phase velocity for the path structure, γ_2 is the frequency dependent attenuation coefficient due to the anelastic structure of the path, and ϕ_0 is the initial phase which is equal to $-3\pi/4$ for an explosion with step function moment. $S_1(\omega)$ and

$S_2(\omega)$ are real functions that depend on the earth structure of the source region and path respectively. $S_1(\omega)$ is positive for a shallow source. Using the notation of Harkrider (1964, 1970),

$$S_1(\omega) = \sqrt{\frac{2A_{R1}}{9\pi\omega c_1^3}} \left[\frac{E_3}{2\mu} - E_1 \right]$$

$$S_2(\omega) = c_2 \sqrt{A_{R2}} \quad (2)$$

E_1 and E_3 are the eigenfunctions of horizontal displacement and normal traction respectively, and are written in Harkrider's notation as $E_1 = \dot{u}_s^*(h)/\dot{w}_0$, $E_3 = \sigma_s^*(h)/(\dot{w}_0/c)$ (μ is the shear modulus at the source). They are functions of the source depth h and the large scale properties of the earth structure. c_1 and c_2 are the phase velocities of the source and path structures, and A_{R1} and A_{R2} are the frequency dependent Rayleigh wave amplitude functions for the source and path regions which depend on the large scale properties of the earth structure.

In the following analysis, the source region elastic structure is assumed to be constrained by independent geophysical evidence and the same structure will be used for all events at a given test site. The quantities which must be determined in Equation (1) are c_2 , S_2 , and γ_2 .

The normalized moment M_0' is equal to $3\beta^2/a^2M_0$, where M_0 is the conventional definition of the moment and a and β are the compressional velocity and shear velocity at the source. For a Poisson solid $M_0 = M_0'$. We define M_0' this way so that it will be a measure of the strength of surface wave excitation by the source, and so the Green's function will be independent of local material properties. With this definition, two nearby explosions in media with different Poisson's ratios will produce surface waves of the same

amplitude if they have the same M_0 , provided that the change in local material properties is not large enough to significantly change the long period eigenfunctions in Equation 2.

III. EXPLOSION DATA FOR THE NEVADA TEST SITE AND EAST KAZAKH

The data used in this study were Rayleigh wave seismograms from underground nuclear explosions at the Nevada Test Site (NTS) and the Soviet East Kazakh test site (EKZ). Stations were selected which had good signal-to-noise ratios for at least two events. The location of the recording stations relative to the test sites are shown in Figures 3, 4, and 5. Twenty-two explosions at the East Kazakh test site were recorded at 12 SRO stations. Forty-eight NTS explosions were recorded at 12 SRO stations and 24 WWSSN stations.

The WWSSN data were hand digitized by ENSCO Incorporated, and installed at the Center for Seismic Studies in Arlington, Virginia. Except for occasional timing errors, we found the WWSSN data to be of very good quality, and we have had little difficulty in applying the inversion procedure to this data. All of the data processing was done on the VAX 11/780 at the Center for Seismic Studies.

The paths shown in Figures 3 through 5 cover a variety of earth structures and a considerable range of distances. The paths from NTS to WWSSN stations are relatively short, ranging from 900 to 4400 km and are all continental paths. The SRO stations are all quite distant from NTS, ranging from 5600 to 14,000 km. Three of these paths are almost entirely oceanic, while the remainder are mixed continental and oceanic. Most of the paths from East Kazakh to SRO stations are between 2000 and 5000 km, but two of the paths are longer than 10,000 km. Seismograms are nearly identical for all events observed along the same path, except for anomalous events with reversed Rayleigh waves.

NTS - WWSSN

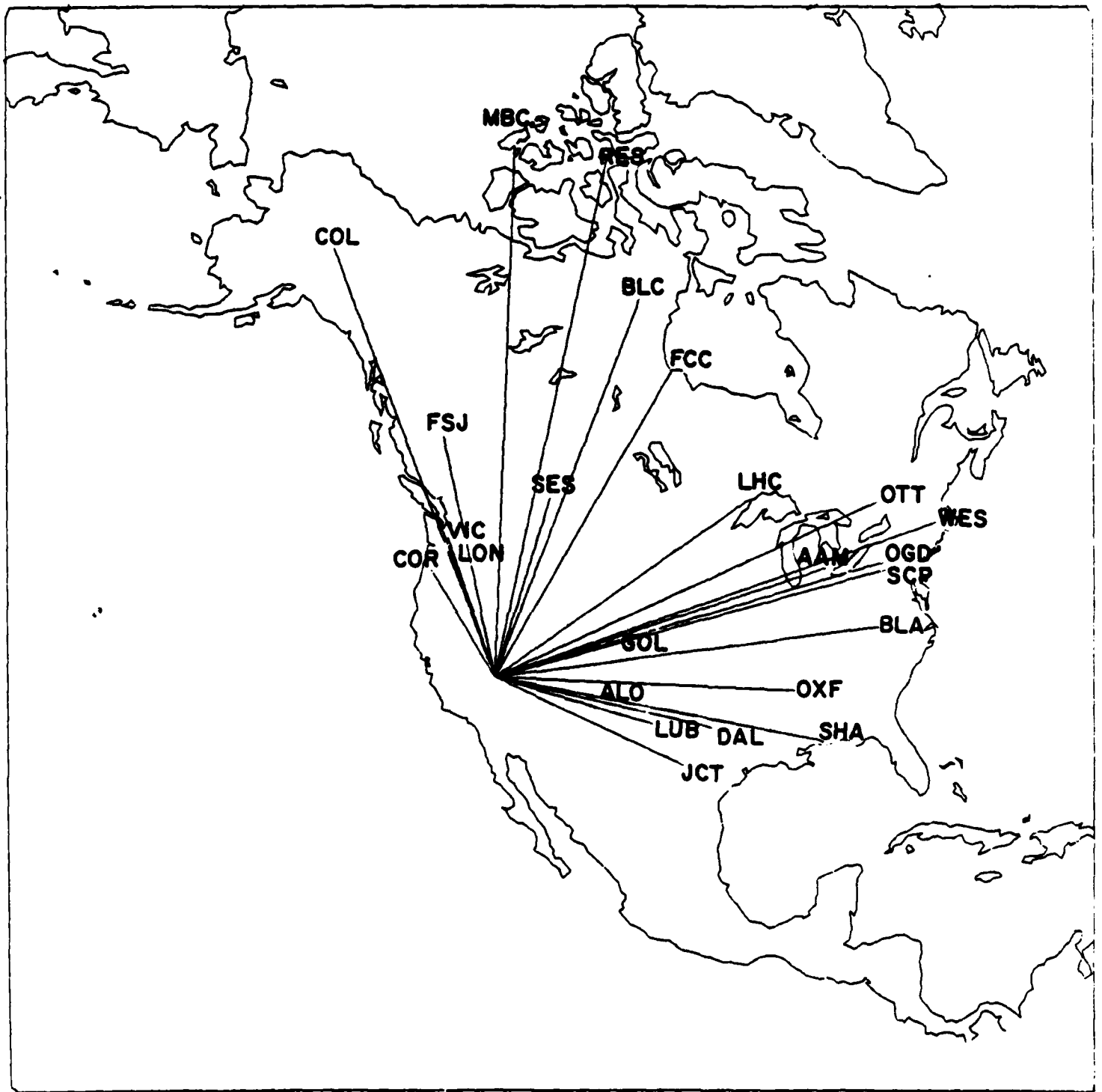


Figure 3. Surface wave paths from NTS to 24 WWSSN stations in the United States and Canada.

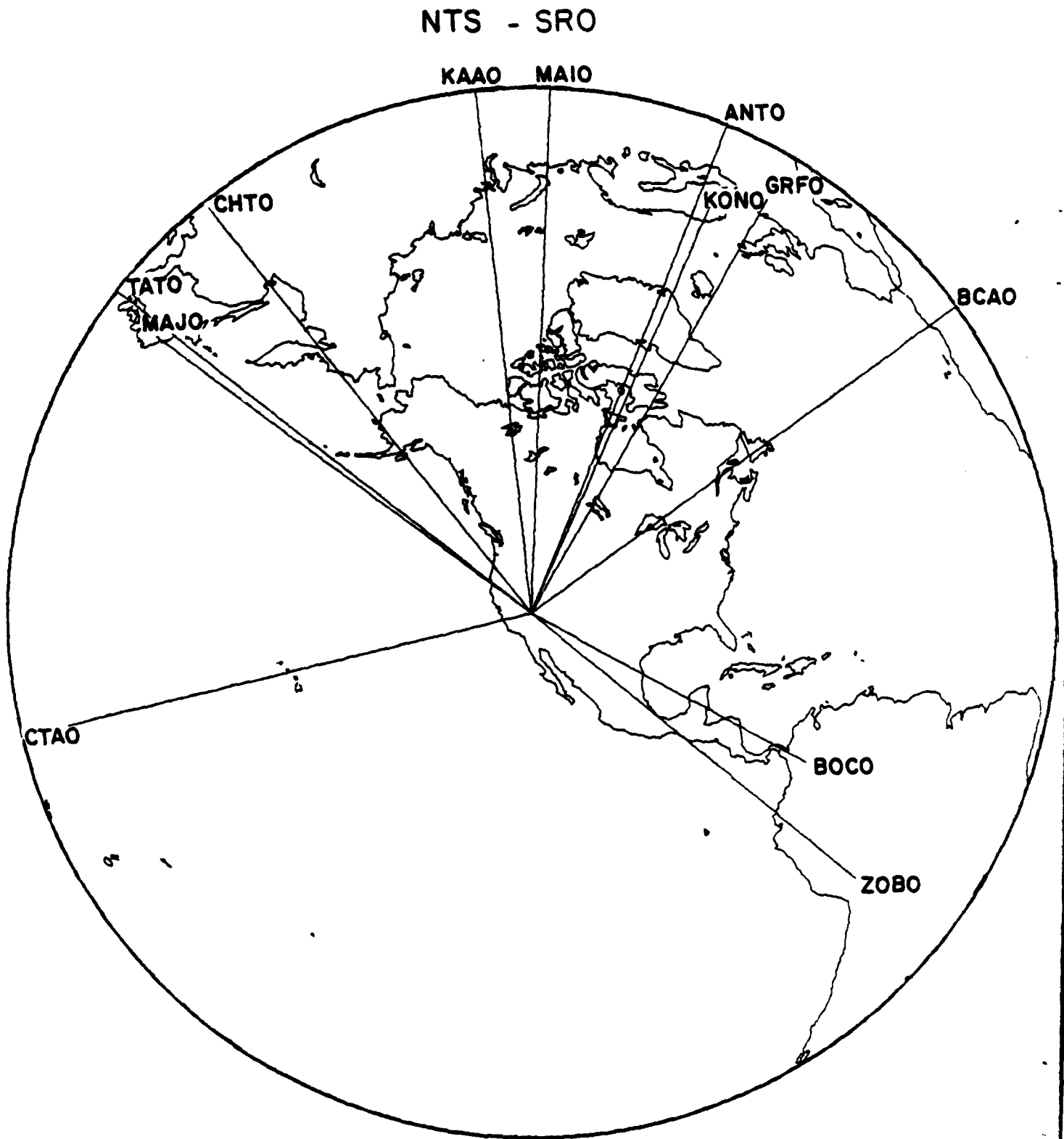


Figure 4. Surface wave paths from NTS to 12 SRO stations. Stations farther than 90 degrees from the test site are shown on the outside of the figure in the direction of the station.

EKZ - SRO

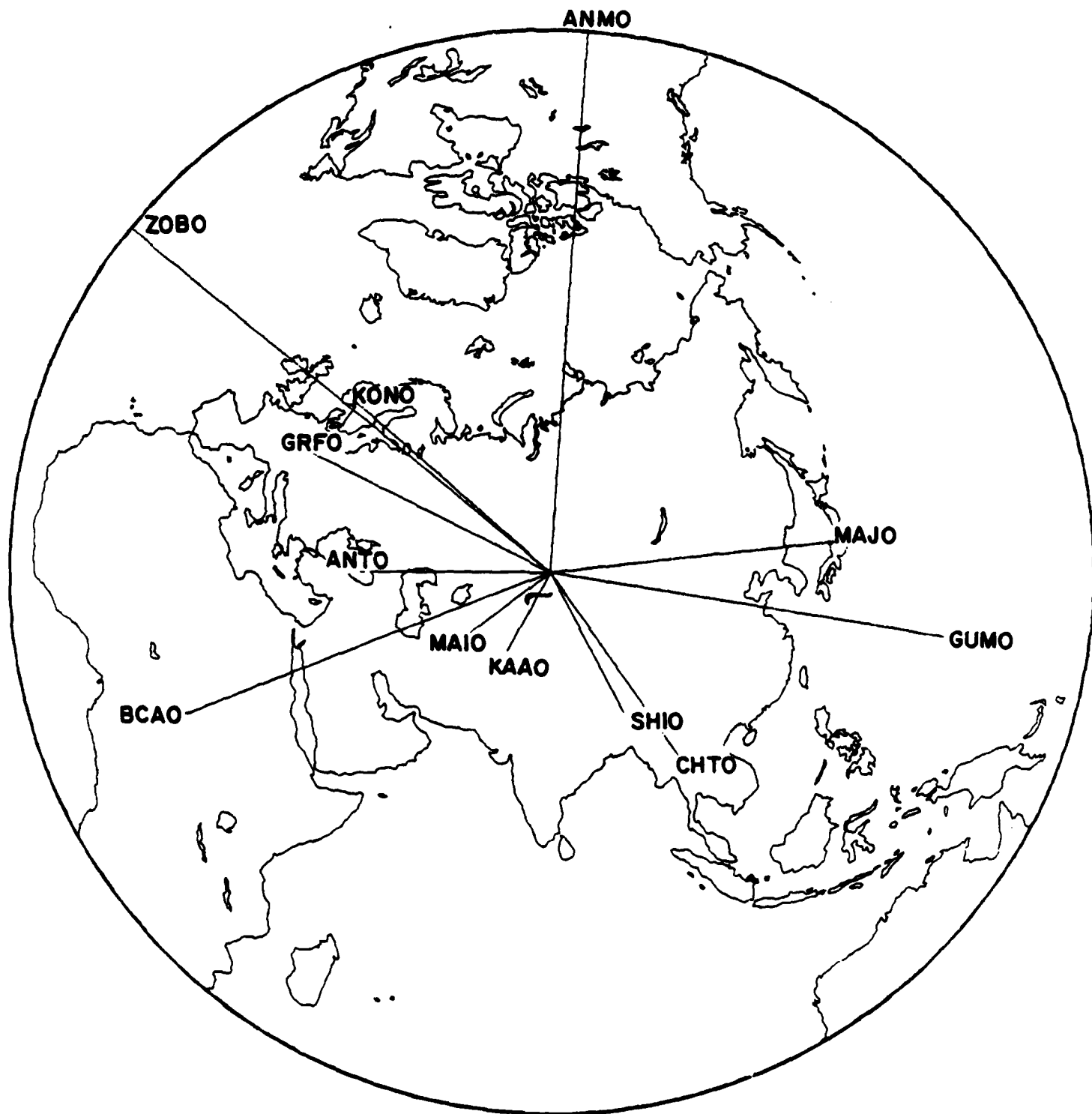


Figure 5. Surface wave paths from East Kazakh to 12 SRO stations.

IV. DATA ANALYSIS AND INVERSION PROCEDURE

A block diagram of the method used for the data processing is shown in Figure 6. We start by finding a set of Rayleigh wave seismograms from a given source region and recorded at the same station which show consistent signals and have good signal-to-noise ratios. We then find the phase velocities, group velocities and amplitude spectra for each of these seismograms using narrow band filtering (Archanbeau, *et al.*, 1966), Dziewonski, *et al.*, 1969, Savino, *et al.*, 1980) and phase-matched filtering (Herrin and Goforth, 1977; Wang, *et al.*, 1981). Group velocities are found first by applying a set of narrow band filters at successive center frequencies and computing the arrival times of the energy envelopes. The phase velocities are found next by integrating the group delays to find the phase as a function of frequency, forming a phase-matched filter, cross-correlating the filter with the seismograms, windowing the compressed signal, and unwrapping the residual phase spectrum to correct the initial phase estimate. We have found that this procedure produces very accurate and consistent measurements of phase velocity. The residual phase is then differentiated to obtain an improved group velocity estimate, and the spectral amplitudes of the Rayleigh waves are found by taking the Fourier transform of the windowed, compressed signal.

After applying this procedure to several seismograms, we check the results to make sure there are no phase-reversed seismograms or other inconsistencies in the dispersion curves. We then average the phase and group velocities and spectral amplitudes for the selected seismograms. This averaging serves three functions - it smooths the data, reduces the chance of error from inaccurate times or locations, and provides standard deviations on the data which are used as weights by the inversion code.

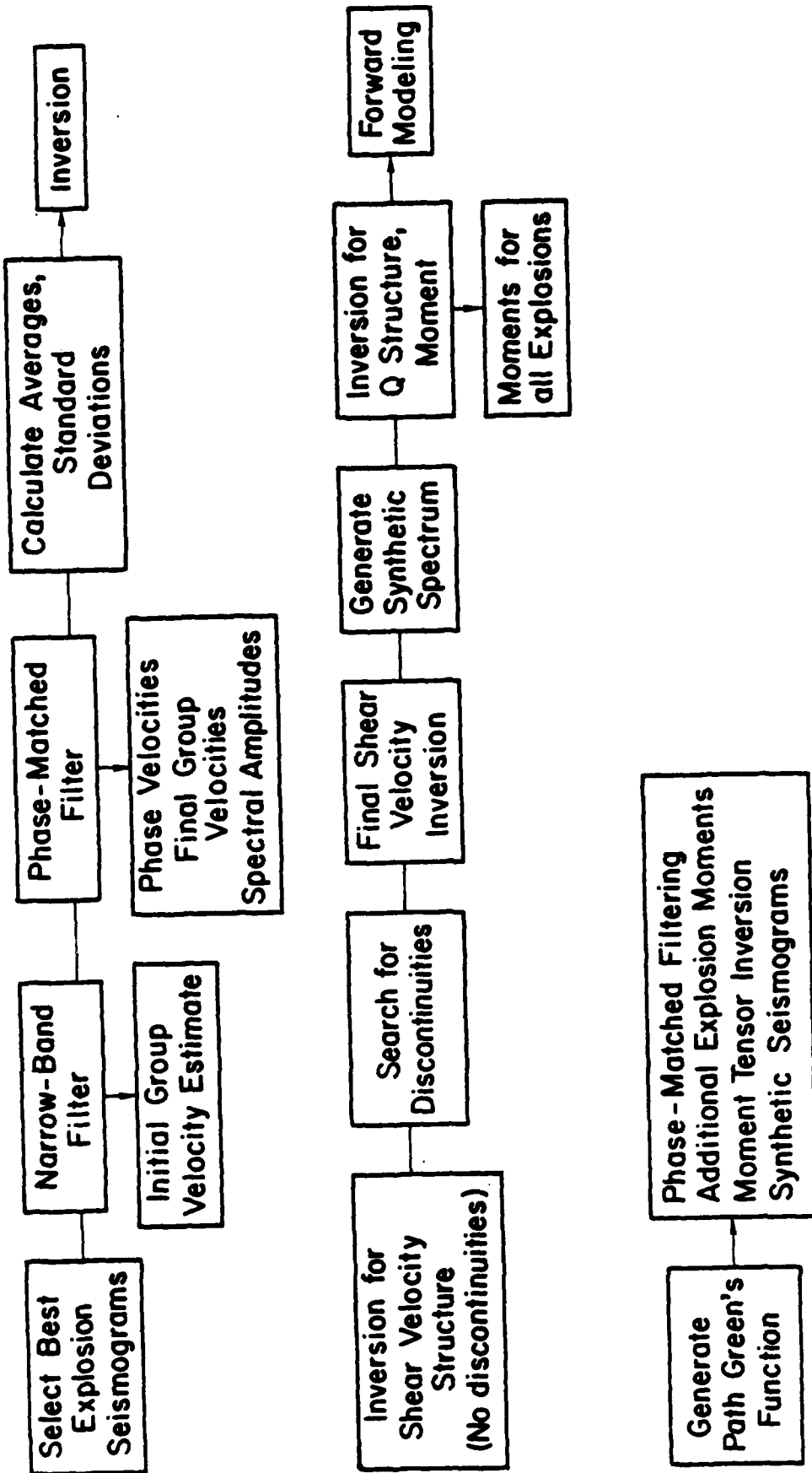


Figure 6. Block diagram of surface wave analysis procedure.

Quality control during path correction processing is very important, and is the most time consuming part of the procedure. The following procedure was used to select the data used for path correction processing. First, the data for each station were plotted and low signal-to-noise ratio data were eliminated (Figure 7). The selected data were replotted and marked at the 3 km/sec group velocity point on the seismograms to help identify timing errors in the data (Figure 8). This step was essential for the hand-digitized WWSSN data. Ten percent of the data was found to contain timing errors. Most of these are minute errors, however, and for these seismograms we simply adjusted the start time by 60 seconds. More troublesome were smaller errors of 10 or 20 seconds. Since we could not easily guess the error in these seismograms, they were not used in the data processing.

Since it was necessary to process a large amount of data (~ 500 seismograms for ~ 50 paths), the interactive procedure described by Stevens, *et al.* (1982) was partially automated. A trial set of input parameters for the data analysis code TELVEL were selected. These parameters are listed in Table 1. The variable parameters are the frequency band and filter Q for narrow-band filtering, the windowing interval for phase-matched filtering, output frequencies, and 2π branch for phase velocity. The phase velocity branch was found by estimating the phase velocity at one frequency and finding the branch closest to this value. The values listed in Table 1 were based on our experience with digital data (where the correct branch can often be found by the long-period behavior), on worldwide average values from Oliver (1962) and on phase velocities measured in the western United States by McEvelly (1964). One seismogram for each path was processed interactively to make sure the input parameters were appropriate.

After the initial processing it is necessary to select the most consistent results and average them for inversion. To check this, we plot all of the phase and group velocity curves to identify

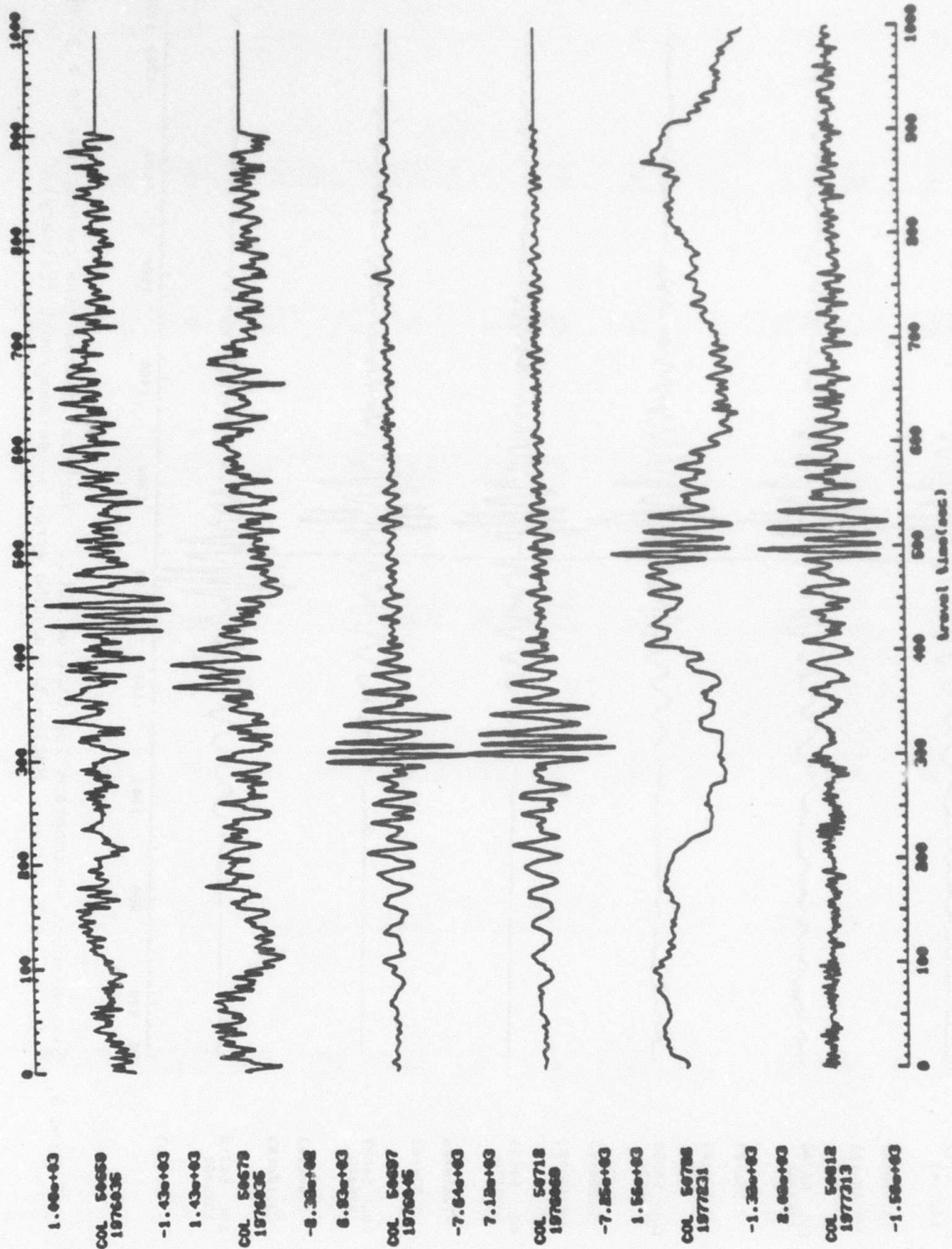


Figure 7. Six seismograms at WWSSN Station COL. Data processing starts by selecting data with good signal/noise ratio. The third and fourth seismograms (explosions Cheshire and Estuary) were used in path correction processing.

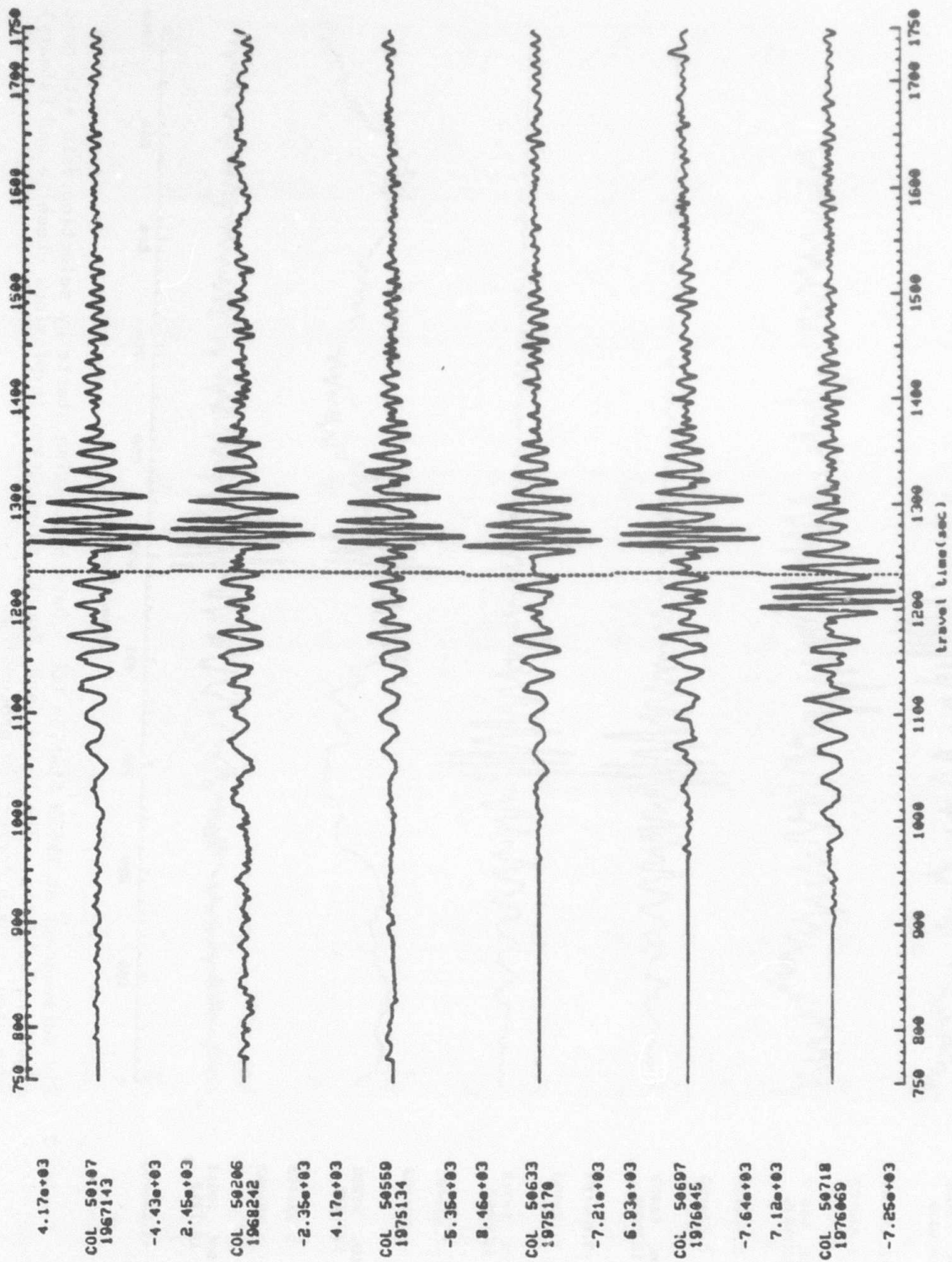


Figure 8. Six selected seismicograms for Station COL. Vertical dashed line corresponds to a group-velocity of 3 km/sec. Notice the minute error in seismogram 6 (Estuary).

TABLE 1
INITIAL PARAMETERS FOR TELVEL

Station Type and Distance	Narrow-Band Filtering			Phase-Matched Filtering Window Half-Width Seconds	Phase- Velocity Branch		Output Frequencies	
	F1	F2	Q	T	F	C	F1	F2
SRD < 5000 km	0.01	0.10	10	75	0.015	4.00	0.0125	0.09
SRD > 5000 km	0.01	0.10	20	75	0.015	4.00	0.0125	0.09
WWSSN < 1250 km	0.01	0.18	8	40	0.040	3.65	0.025	0.15
WWSSN < 2750 km	0.01	0.15	10	50	0.030	3.80	0.020	0.125
WWSSN > 2750 km	0.01	0.15	12	60	0.020	3.95	0.015	0.125

inconsistent data. There is almost always some bad data resulting from interference, digitization errors, phase reversals, incorrect phase velocity branches, or timing errors. In the upper figure in Figure 9, we show phase and group velocities for all seismograms processed at Station LON. Three seismograms were rejected on the basis of the figure. The phase velocity curve which is offset from the rest resulted from a 10 second timing error. The two curves which are inconsistent at long-periods are the result of digitization errors. This is a common problem in hand-digitized data when there is a strong Airy phase - narrow-band filtering finds the Airy phase even at the longest periods, so a nearly constant group velocity curve results. We have never seen this effect in digital data. The lower figure shows the average phase and group velocities together with \pm one standard deviation curves for the remaining nine seismograms at Station LON.

In Figure 10, we show the final phase and group velocities found for NTS to WWSSN stations, NTS to SR0 stations, and East Kazakh to SR0 stations. The phase and group velocities are very consistent for different events observed along a given path. Typical phase velocity standard deviations are 0.1 to 0.2 percent, while group velocity standard deviations are a few tenths of a percent. The standard deviations of all quantities increase near the ends of the observable frequency band, and also near spectral dips.

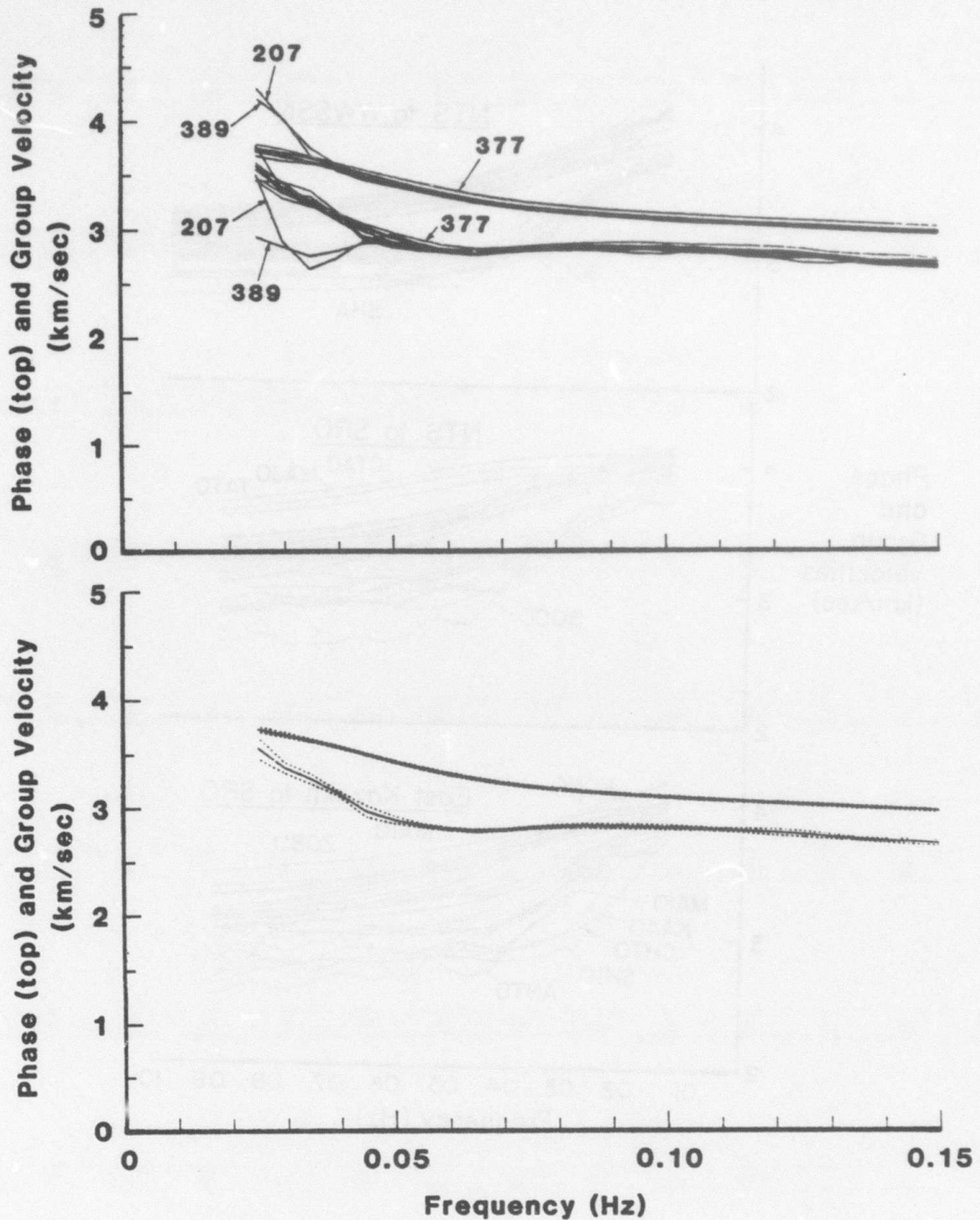


Figure 9. Phase and group velocities for path from NTS to LON (1155 km). top figure shows velocities for each seismogram. Bottom figure shows average (solid) and $\pm 1\sigma$ curves after deleting data with timing and digitization errors. Origin id numbers are marked for inconsistent events.

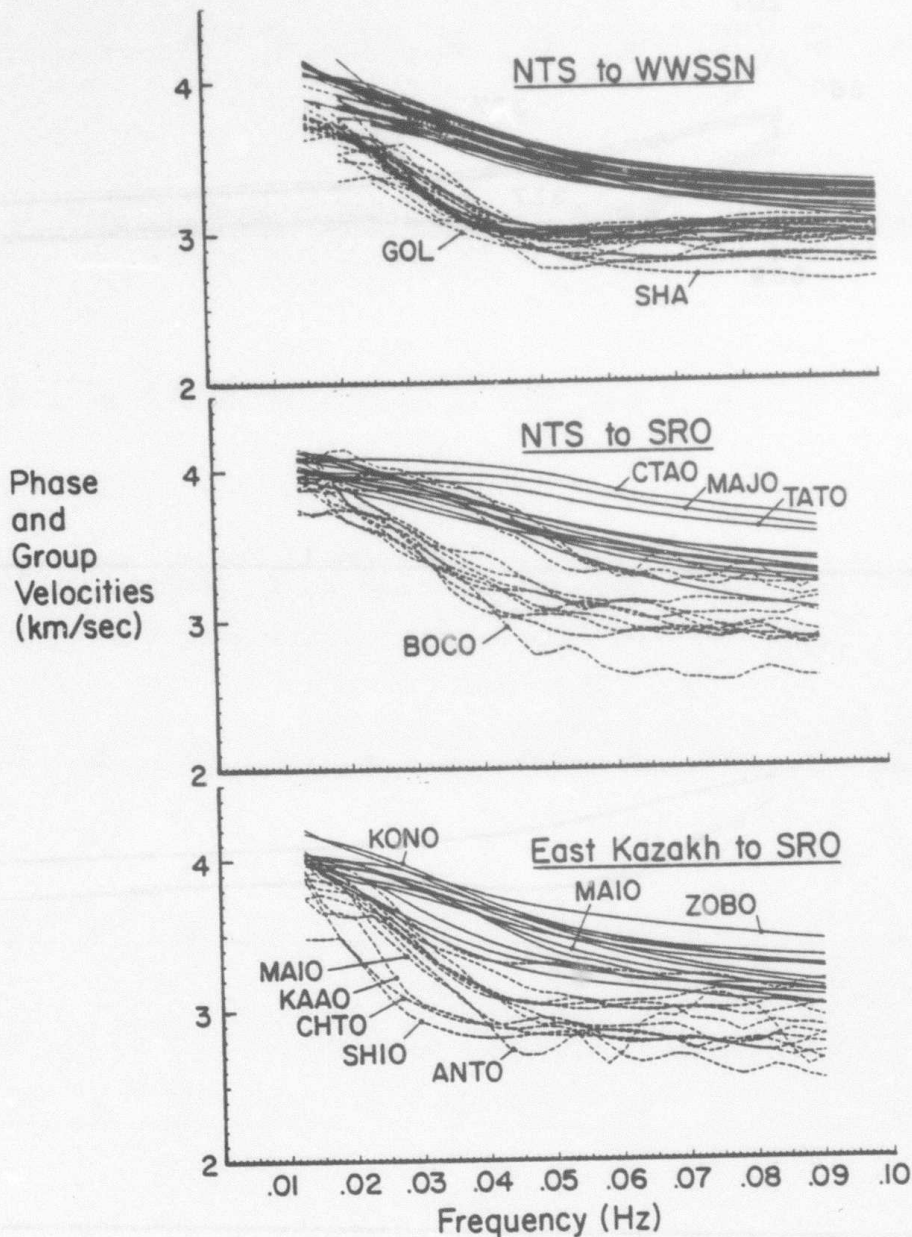


Figure 10. Phase and group velocities for paths from NTS to WWSSN stations (top), NTS to SRO stations (middle) and East Kazakh to SRO stations (bottom). Solid lines are phase velocities; dashed are group velocities. The three paths with high phase velocity in the NTS to SRO figure are predominantly oceanic paths. The three dispersion curves with very low group velocities at 0.03 Hz in the East Kazakh figure correspond to the paths with thick, low velocity crusts to the south of the test site.

V. INVERSION FOR SHEAR VELOCITY STRUCTURE

The shear velocity structure is found by simultaneously inverting the phase and group velocities. The method used is similar to the method used by Bache, *et al.* (1978a). The inversion program attempts to fit the data with a smooth model by minimizing the integral of $|d\beta/dz|$ over the structure, except across discontinuities at depths specified by the user. The inversion method is iterative, with the inversion model for each iteration becoming the starting model for the next iteration. The final results are completely independent of the starting model, and the initial starting model is necessary only to allow the calculation of partial derivatives of phase and group velocities with respect to model parameters.

Inversion is performed for shear velocity only, as there is not enough information in the fundamental mode phase and group velocities to determine the compressional velocities and densities at the same time. We use data on crust and upper mantle properties from Dobrin (1976) to constrain these parameters. Compressional velocity is constrained to be consistent with a Poisson's ratio of 0.27, while density is constrained by a Birch's law given by $\rho = 0.65\beta + 400$ (in MKS units).

A 20 layered model is used for the inversion. The thickness of the layers and depth of the model are derived from the frequency content of the data. The maximum depth is approximately equal to the longest wavelength c/f , and layers are thickest near the maximum depth and become thinner near the free surface. The inversion is damped, so that the model chosen has approximately five or six degrees of freedom depending on the quality of the data. This allows an excellent fit to the data in most cases, and produces a smooth model free of the spurious oscillations which would result from allowing more degrees of freedom.

Discontinuities in the structure are explicitly allowed at the crust-mantle boundary and in some cases at shallower depths to allow for near surface sedimentary layers. The depths of the discontinuities are found in the following way. We first perform an inversion to find the best model with no discontinuities. Then we insert discontinuities at each layer boundary, invert, and search for minima in the resulting data misfit. Discontinuities are inserted at these depths, and a final inversion is performed with the discontinuities included.

In Figure 11, we show the data misfit minima found using the initial structure (with no discontinuities) shown in Figure 12. Data misfits are shown for several degrees of freedom. The data misfit is normalized to the standard deviations on the data, so a data misfit of 1.0 means that the average misfit between the calculated and observed phase and group velocities is one standard deviation. Minima are found close to 7.5 km and 40 km, so discontinuities are inserted at these depths. The final model is also shown in Figure 12.

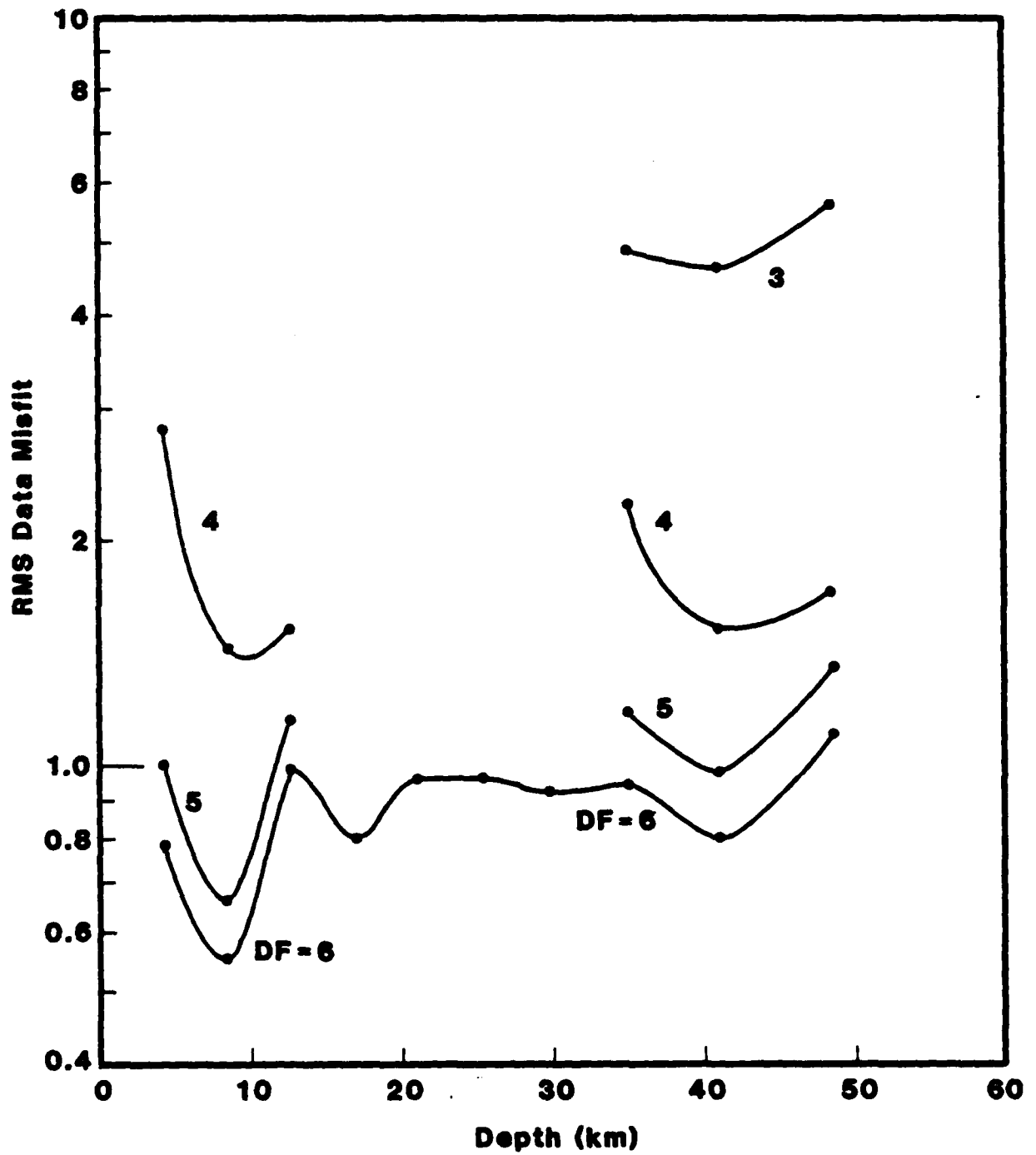


Figure 11. Data misfit minima for NTS-AAM. Discontinuities were inserted after each layer. Minima in data misfit correspond to discontinuities in structure. Curves are marked for different degrees of freedom. The final structure (see next figure) has discontinuities at 7.5 and 40 km.

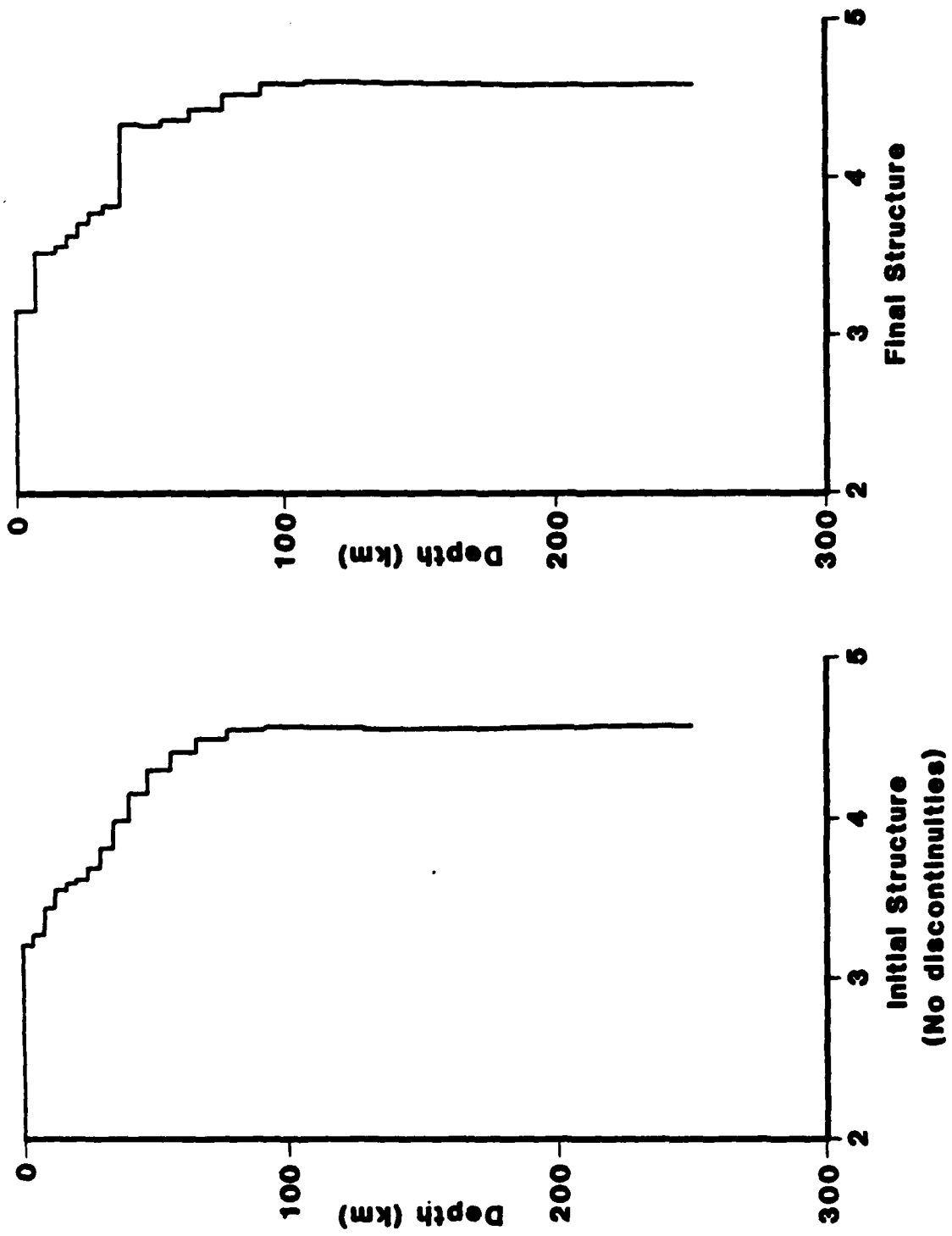


Figure 12. Initial and final shear velocity structures for path NTS--AAM.

VI. INVERSION FOR Q STRUCTURE AND SCALAR MOMENT

The final step in the inversion procedure is the inversion of the average spectral amplitude for Q and moment. The average spectral amplitude is the linear average of the spectra of the best events recorded for a given path, defined by

$$u(\omega) = \frac{1}{N} \sum_{i=1}^N u_i(\omega) \quad (3)$$

where u_i are the individual spectra and N is the number of frequencies. The relative moments of the individual spectra may be found using the least squares relation

$$M_i^r = \frac{\sum_{\omega} u(\omega) u_i(\omega)}{\sum_{\omega} u(\omega) u(\omega)} \quad (4)$$

so once the absolute moment corresponding to the average spectrum is determined, the moments of all the events are determined. Standard deviations on the normalized spectra (spectra divided by their relative moments) are used as weights in the inversion. The standard deviations are defined by

$$\sigma^2(u(\omega)) = \frac{1}{N-1} \sum_{i=1}^N \left[u(\omega) - \frac{1}{M_i^r} u_i(\omega) \right]^2 \quad (5)$$

In Figure 13, we show the spectra of individual seismograms and the average spectrum with standard deviations for the path from NTS to Station LON.

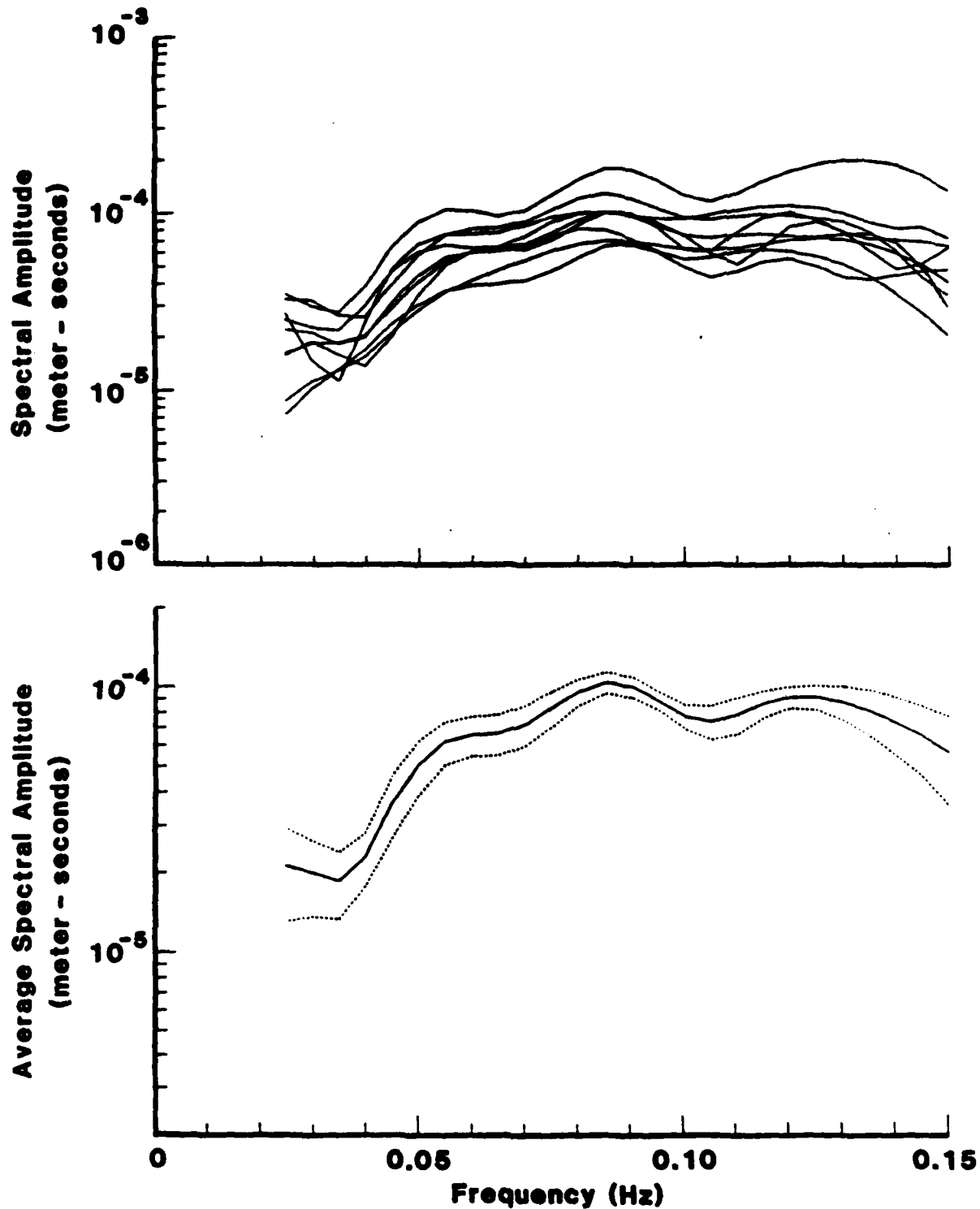


Figure 13. Spectral amplitudes for NTS-LON path. Top figure shows individual spectra for nine explosions. Bottom figure shows average spectra and standard deviation as defined in the text.

Rewriting Equation (1), we define the data used for the inversion to be the ratio between the synthetic spectral amplitude $S(\omega)$ (for unit moment, without including attenuation) and the observed amplitude spectrum $u(\omega)$:

$$\frac{1}{r} \ln \frac{S(\omega)}{u(\omega)} = \gamma(\omega) - \frac{1}{r} \ln M_0' \quad (6)$$

$S(\omega)$ is defined by

$$S(\omega) = S_1(\omega)S_2(\omega)/\sqrt{a_e \sin(r/a_e)} \quad (7)$$

The attenuation coefficients $\gamma(\omega)$ can be expanded in terms of the Q structure of the path using the phase velocity partial derivatives (Mitchell, 1975; Anderson, et al., 1965). Q is assumed to be depth dependent, but frequency independent. Explicitly, assuming no bulk losses

$$\gamma(\omega) = \frac{\omega}{2c^2} \sum_{i=1}^N \left(\frac{\partial c}{\partial \beta_i} + \frac{4}{3} \frac{\beta_i}{a_i} \frac{\partial c}{\partial a_i} \right) \frac{\beta_i}{Q_i} \quad (8)$$

where the index i indicates the layer in the inversion model and N is the total number of layers. a_i , β_i , and Q_i are the compressional velocity, shear velocity and Q , respectively, in each layer.

In the Q /moment inversion, the amplitude of the spectral ratio in Equation (6) determines the moment, while the shape determines the Q structure. We use a smoothness criterion, as in the inversion for shear velocity structure to damp oscillations in the solution. Since there is some correlation between low velocity zones and low Q zones in the earth, we invert for β/Q , and find the smoothest β/Q structure

consistent with the data. The Q /moment inversion is less robust than inversion for structure, since there is an additional free parameter (the moment) and since spectra are less smooth than dispersion curves. As a result, the solution must be more heavily damped by allowing fewer degrees of freedom in the inversion. The minimum number of degrees of freedom is two - one to determine the moment and one to find the average β/Q value for the path. With exactly two degrees of freedom, Q in each layer is proportional to the shear velocity, with the proportionality constant determined by the inversion. More degrees of freedom allow more shape in the Q structure.

We impose one additional constraint on the Q inversion. Tests on synthetic seismograms show that while the Q inversion procedure accurately reproduces the Q structure of the crust, lower Q zones beneath the crust are not well resolved, and the Q at depth is usually overestimated. This causes the moments measured at distant stations to be underestimated. We can reduce this problem by including an estimated value for the average mantle Q at depth as a data point. With this constraint, the Q inversion is stable and physically reasonable Q structures are obtained with an inversion that allows approximately 3.5 degrees of freedom in the model.

VII. SHEAR VELOCITY INVERSION RESULTS

Several representative shear velocity structures obtained by inversion are shown in Figure 14. Three continental and one predominantly oceanic structures are shown for NTS. The continental structures are all quite similar. The path to SHA has unusually low velocities in the upper few kilometers. Note the corresponding low group velocities for this path in Figure 10. The path from East Kazakh to KON0 crosses a stable, relatively fast shield structure. The path to MAJO is similar, but somewhat slower and more complex. The path to SHIO crosses the Tibetan plateau, and the inferred structure has a thick, low velocity crust. The path to ANTO has low velocities in the upper part of the crust.

Our main interest here is in the effect of these structures on surface wave amplitudes. In Figure 15, we show the path amplitude functions S_2 calculated using all of the path structures. The elastic structure of the source-to-receiver path has surprisingly little effect on the spectral amplitudes. The maximum variation in $\log(S_2)$ is only 0.15 at 20 seconds. The paths with the largest values of S_2 are the thick crust, low velocity paths, while the smallest values occur along oceanic paths.

These results mean that the surface wave amplitudes are not changed very much by the elastic properties of the travel path. This is, of course, only true for spectral amplitudes, not for time domain amplitudes. Differences in dispersion can cause large differences in time domain surface wave amplitudes, especially at distances less than 30 degrees. On long or complex paths, when a plane-layered model is not a good approximation, interference will cause more spectral amplitude variation than is predicted by the smooth functions in Figure 15.

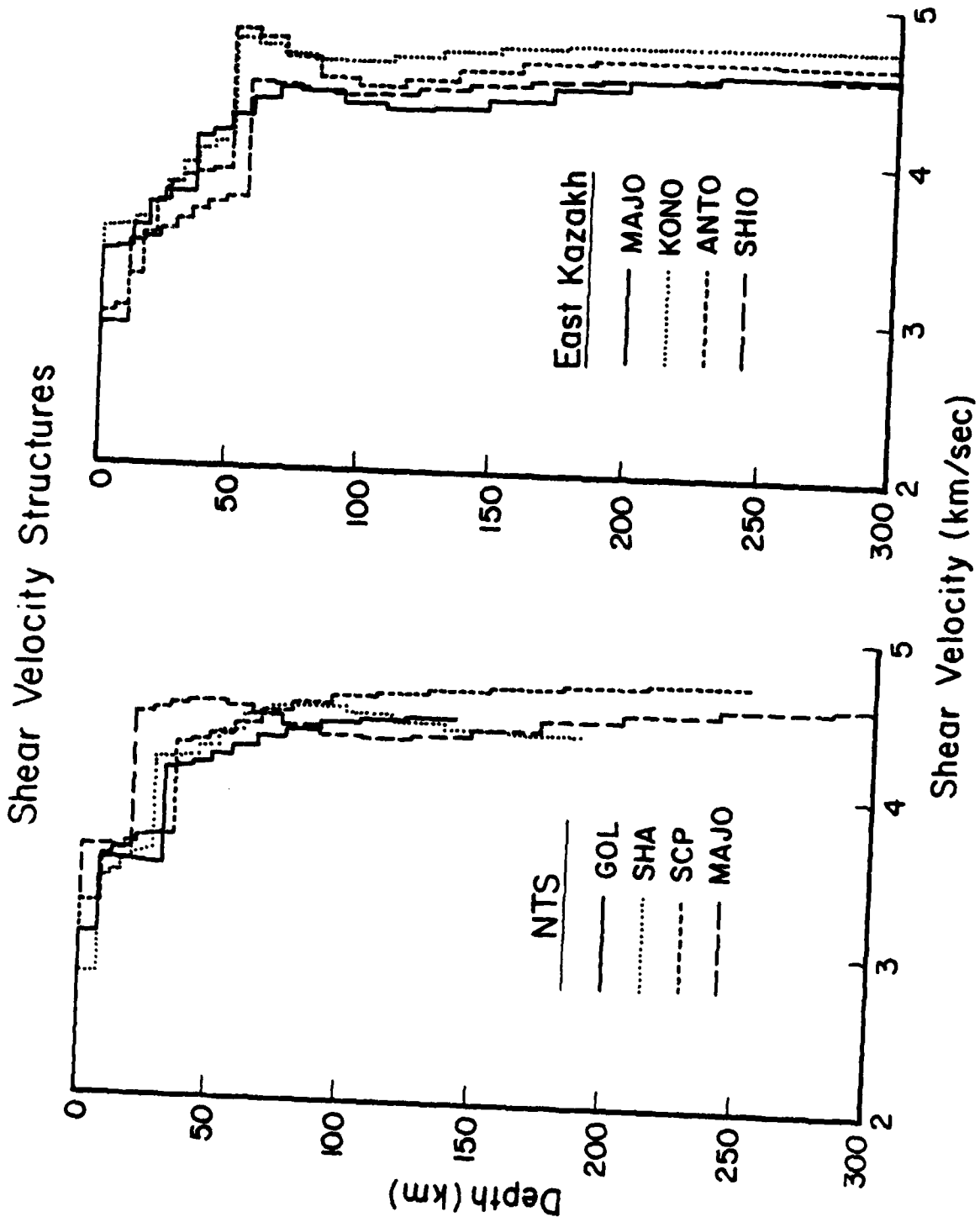


Figure 14. Shear velocity structures obtained by inversion for selected paths.

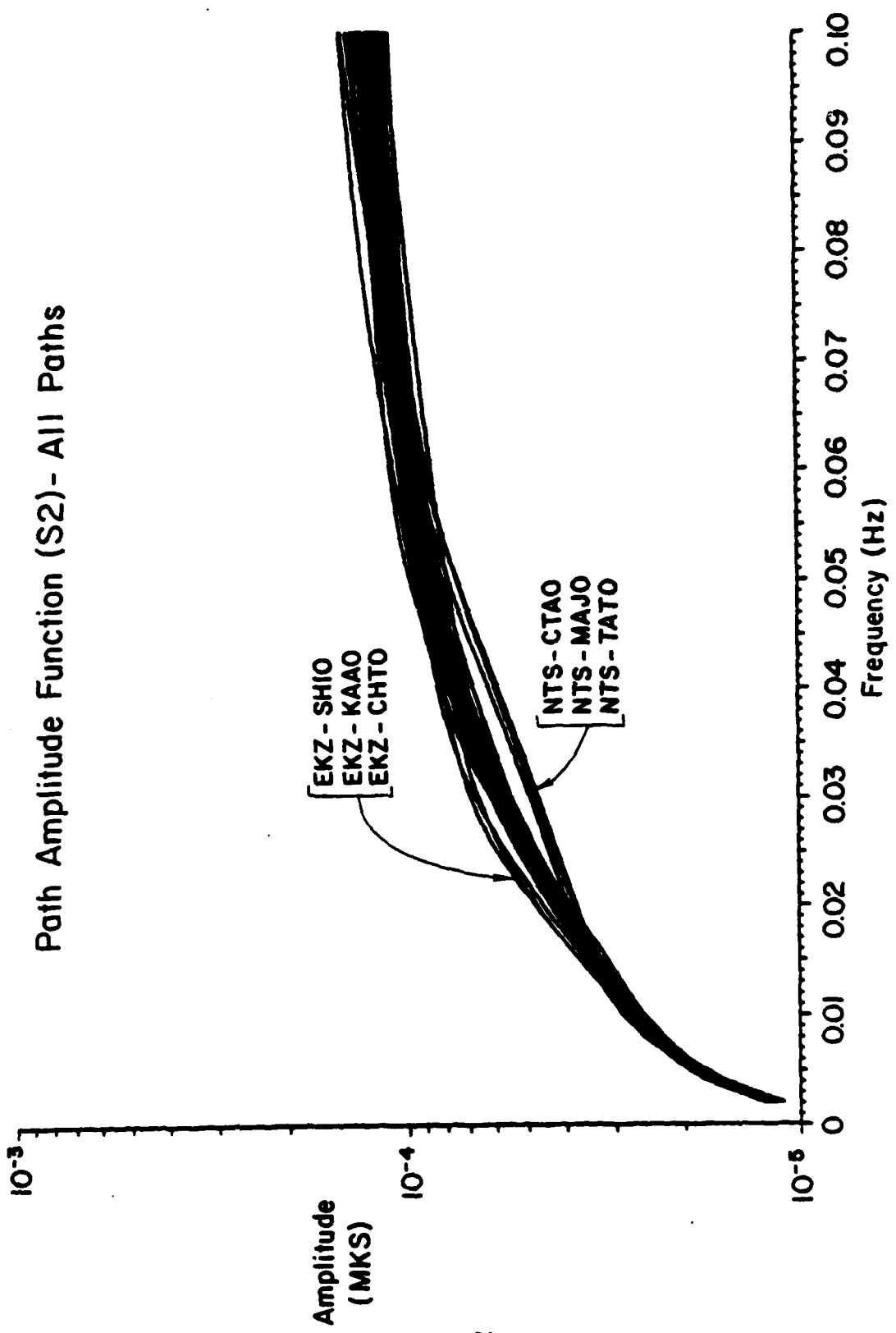


Figure 15. Path amplitude function S_2 for all paths from NTS and East Kazakh.

VIII. Q CONSTRAINTS AND INVERSION RESULTS

To invert for the path Q structures and the explosion moments, we need the excitation function S_1 for the source region structures, and an estimate of mantle Q at depth to be used as a constraint.

The Soviet test site is located in the Kazakh Fold System near latitude 50 degrees north and longitude 79 degrees east. According to Beliayevsky, *et al.* (1968), the results of a deep seismic sounding survey show that the average crustal thickness in the area is 50 km. Close to the test site, however, the crustal thickness decreases to about 45 km. Compressional velocities in the crust are very similar to velocities in the stable shield and platform regions of the Eurasian continent, except for the absence of low velocity surface sediments in the Kazakh Fold System. Grand, *et al.* (1984) show that the shear velocity in the crust near the source region is relatively slow, similar to the shear velocity of the platforms to the south and east, but slower than the velocity along the shield paths to Europe.

For our model of the East Kazakh source region, we use a modification of the structure inferred for the path to MAIO. This path crosses the Turanian Plateau southwest of the test site. The crustal thickness of this structure is 45 km. We have increased the inferred velocities in the top 15 km (see Figure 16) to remove the influence of the low velocity sediments in the plateau. The structure in the upper crust is then consistent with velocities from Beliayevsky, *et al.* (1968). We have reduced the velocity in the top 1.5 km to 5.0 km/sec (compressional) and 2.7 km/sec (shear) with a density of 2.7 gm/cm³. These values are appropriate for weathered hard rock such as granite.

East Kazakh Source Region Structure

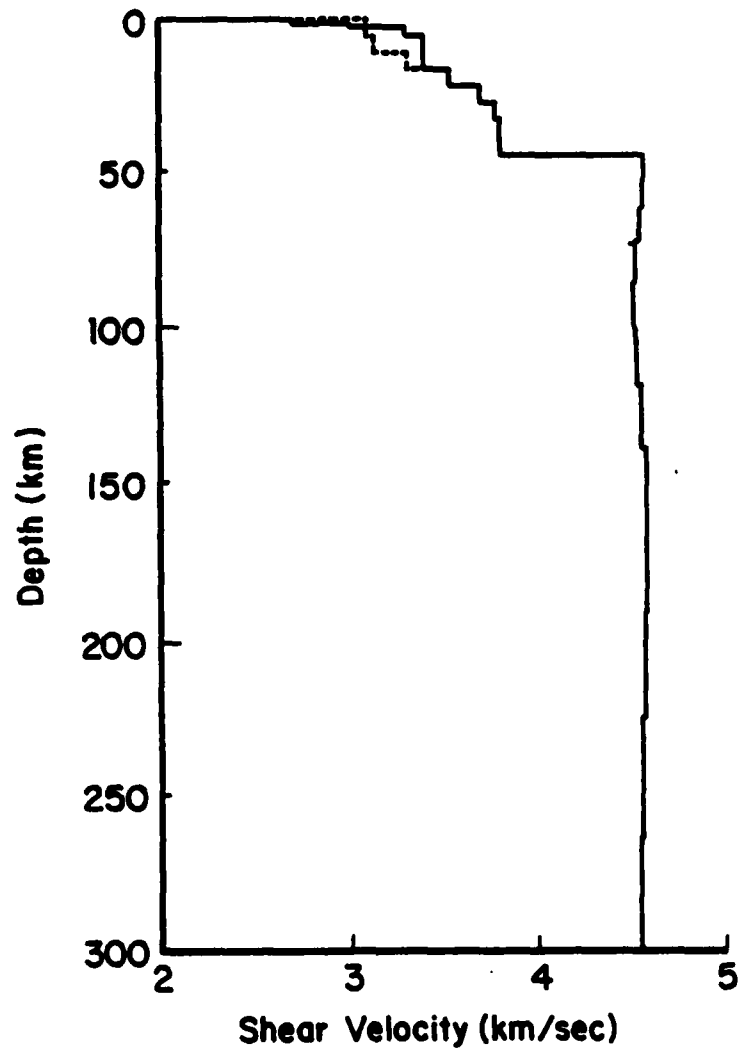


Figure 16. Source region structure used for the East Kazakh test site. The structure found for East Kazakh to MAIO (dashed line) was modified to construct the East Kazakh structure.

The models used for NTS and East Kazakh are listed in Tables 2 and 3 and shown in Figure 17. The NTS model is based on the NTS-TUC crustal structure of Bache, *et al.* (1978a), merged with the upper mantle structure of Anderson and Hart (1976, 1978). The shallow structure (upper 4 km) is the Pahute Mesa structure from Bache, *et al.* (1975). The shear velocity at the source depth of 1 km is 2000 m/sec, and the shear velocity in the top 500 m is 1000 m/sec.

The excitation functions for the two source regions are shown in Figure 18. The excitation function for NTS is greater than the excitation function for East Kazakh at all frequencies of interest, and particularly at higher frequencies. We therefore expect an explosion at NTS to generate larger surface waves than an explosion at East Kazakh with the same moment.

We also need an estimate of worldwide average mantle Q to use as a constraint on the inversions, so we have searched through the literature to find a representative set of Q estimates. Anderson and Hart (1978) find a worldwide average Q of 90 to 110 between 80 and 300 km depth. Canas and Mitchell (1978) find a minimum mantle Q of 100 to 200 in the Pacific Ocean with the minimum at about 150 km depth, while Canas and Mitchell (1981) find a minimum mantle Q of 60 to 150 in the Atlantic Ocean at 100 to 150 km depth. Cara (1981) finds a mantle Q of 80 to 100 between 100 and 300 km depth for paths across the Pacific Ocean. Lee and Solomon (1979) find very low mantle Q values of about 20 in the Western United States between 80 and 160 km, 25 in the east-central United States below 135 km, and 70 in the Central Pacific below 60 km. Singh (1982) finds a mantle Q of about 50 in southern Asia. Patton (1980) finds mantle Q values of 60 to 150 in western Eurasia at depths below 50 km, 100 to 150 in eastern Eurasia at depths below 100 km, and 300 to 500 in the stable platforms of Eurasia at depths below 50 km. There is a considerable amount of uncertainty in all of these results, and considerable variation in the estimates.

TABLE 2
NTS SOURCE REGION STRUCTURE

Thickness (km)	P-Velocity (km/sec)	S-Velocity (km/sec)	Density (g/cm ³)
0.5	2.00	1.00	1.70
1.0	3.30	2.00	2.10
1.5	4.50	2.70	2.40
1.0	5.90	3.40	2.75
8.0	5.96	3.52	2.78
9.0	6.11	3.61	2.80
10.0	6.37	3.76	2.84
14.0	7.90	4.42	3.20
20.0	8.05	4.50	3.30
15.0	8.10	4.50	3.30
40.0	8.00	4.40	3.30
30.0	7.90	4.30	3.25
30.0	7.90	4.30	3.25
40.0	8.00	4.40	3.30
"	8.50	4.70	3.50

TABLE 3
EAST KAZAKH SOURCE REGION STRUCTURE

Thickness (km)	P-Velocity (km/sec)	S-Velocity (km/sec)	Density (g/cm ³)
1.5	5.00	2.70	2.70
1.0	5.40	3.00	2.70
3.0	5.90	3.30	2.70
11.0	6.10	3.40	2.70
5.5	6.31	3.54	2.70
5.5	6.60	3.70	2.81
5.5	6.74	3.78	2.86
5.6	6.78	3.81	2.88
6.5	6.80	3.81	2.88
8.0	8.15	4.57	3.37
9.4	8.14	4.57	3.37
10.9	8.11	4.55	3.36
12.8	8.06	4.53	3.34
15.0	8.05	4.52	3.34
17.5	8.07	4.53	3.35
20.4	8.12	4.56	3.36
23.9	8.15	4.58	3.38
27.9	8.16	4.58	3.38
32.6	8.15	4.58	3.37
38.2	8.12	4.56	3.36
"	8.10	4.55	3.36

Source Region Elastic Structure

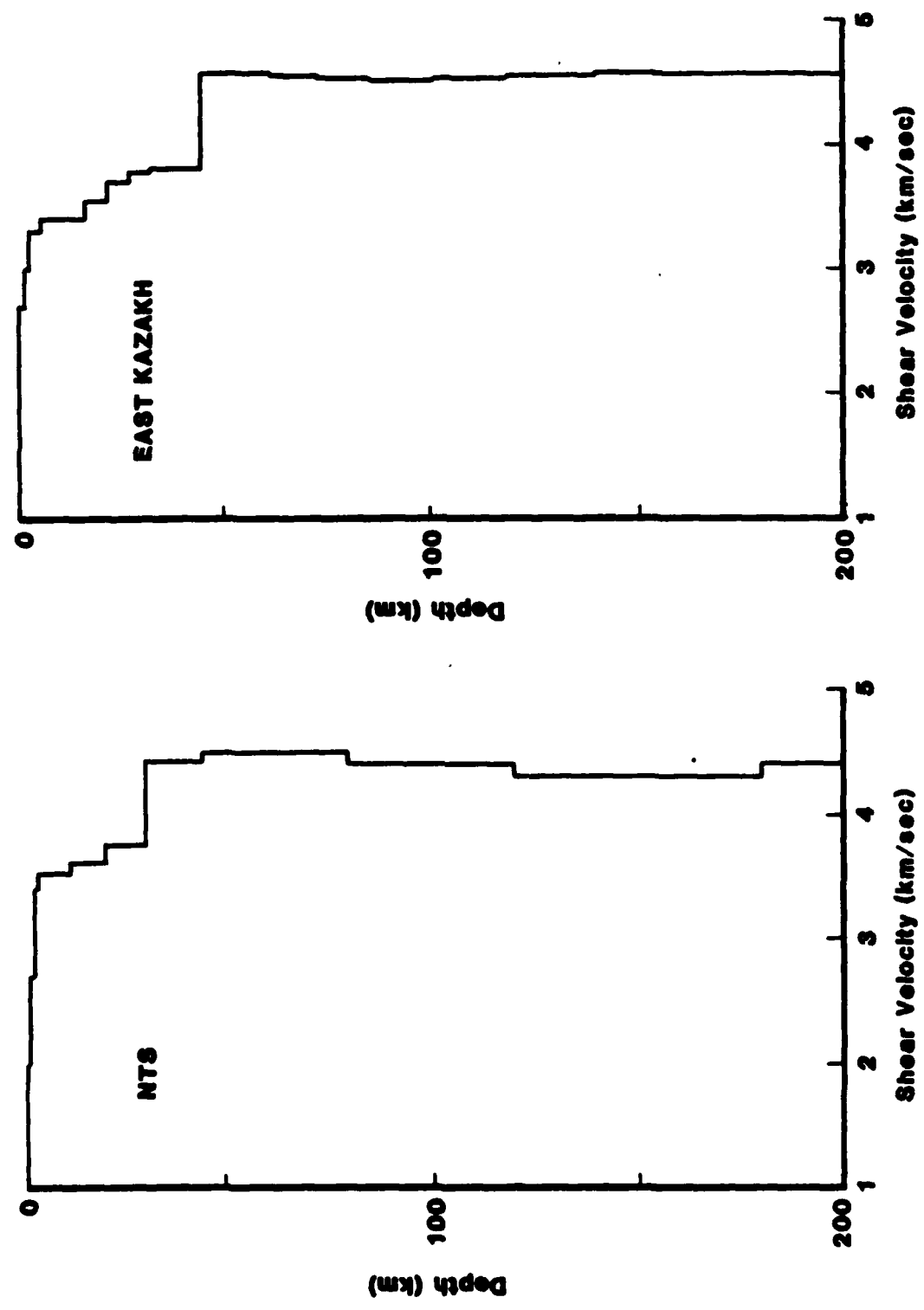


Figure 17. Source region shear velocity models used for NTS and East Kazakh.

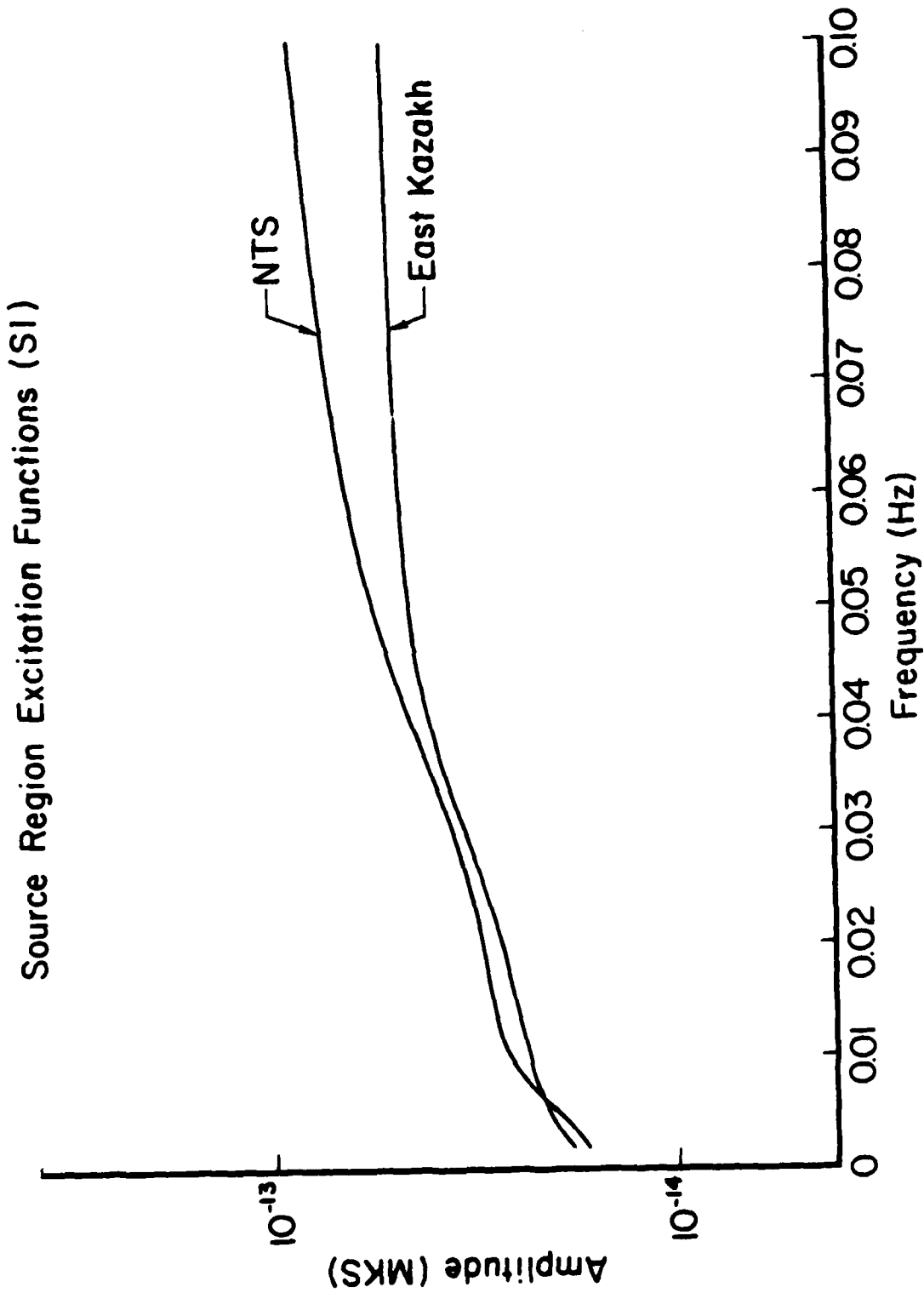


Figure 18. Excitation functions calculated at a depth of 1 km using the NTS structure and the East Kazakh structure.

In the inversions described in this paper, we set β/Q equal to 40 with a standard deviation of 1 between 120 and 150 km depth. Since the shear velocity at this depth is between 4000 and 5000 m/sec, Q is constrained to be slightly more than 100 in this depth range. The inversion algorithm treats this "constraint" as a data point and tries to find a Q structure that both fits the observed spectral amplitude data and has the preferred Q value in the specified depth range. The Q value from the inversion may vary from the preferred value if the data requires it.

Several representative Q structures are shown in Figure 19. Inferred crustal Q is quite variable, with very low values for some complex paths such as East Kazakh to ANTO in Turkey. Seismograms recorded at KONO (from East Kazakh) are rich in high frequencies, which may imply a high crustal Q along this path.

In Figure 20, we show the inferred attenuation coefficients for all paths. In Table 4, we have listed the average 20 second values of attenuation coefficients, together with the structural parameters, for paths from NTS to WWSSN stations and SRO stations, for the three oceanic paths out of NTS, for paths from East Kazakh to SRO stations and for all paths. Differences in attenuation may be responsible for large amplitude variations. Rayleigh waves observed along paths with attenuation coefficients of $1.0 \times 10^{-7}/\text{meters}$ and $3.0 \times 10^{-7}/\text{meters}$ (the \pm one standard deviation values for all paths) will differ by 0.09 magnitude units at 1000 km, 0.43 magnitude units at 5000 km, and 0.87 magnitude units at 10,000 km.

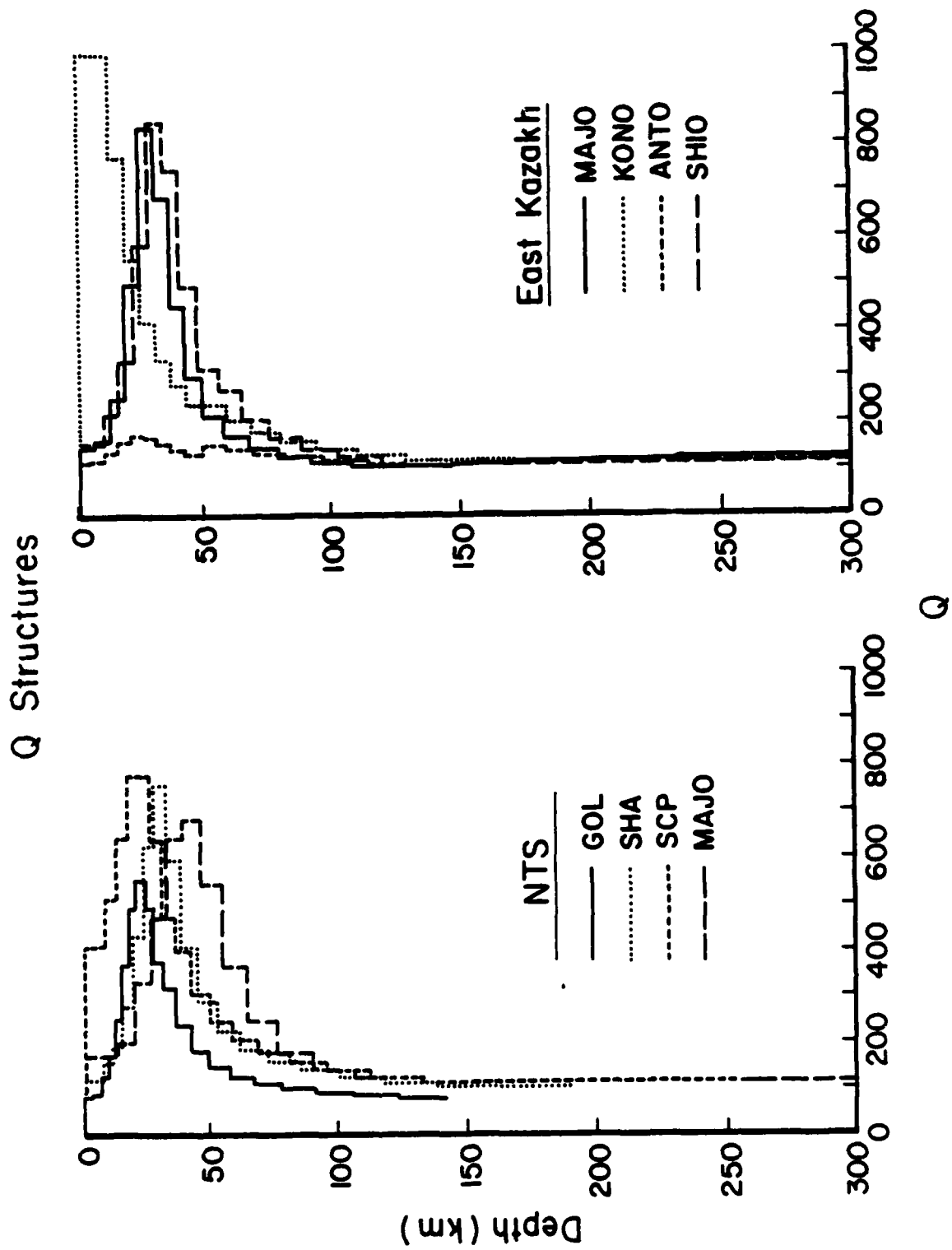


Figure 19. Q structures found by Q/moment inversion for selected paths.

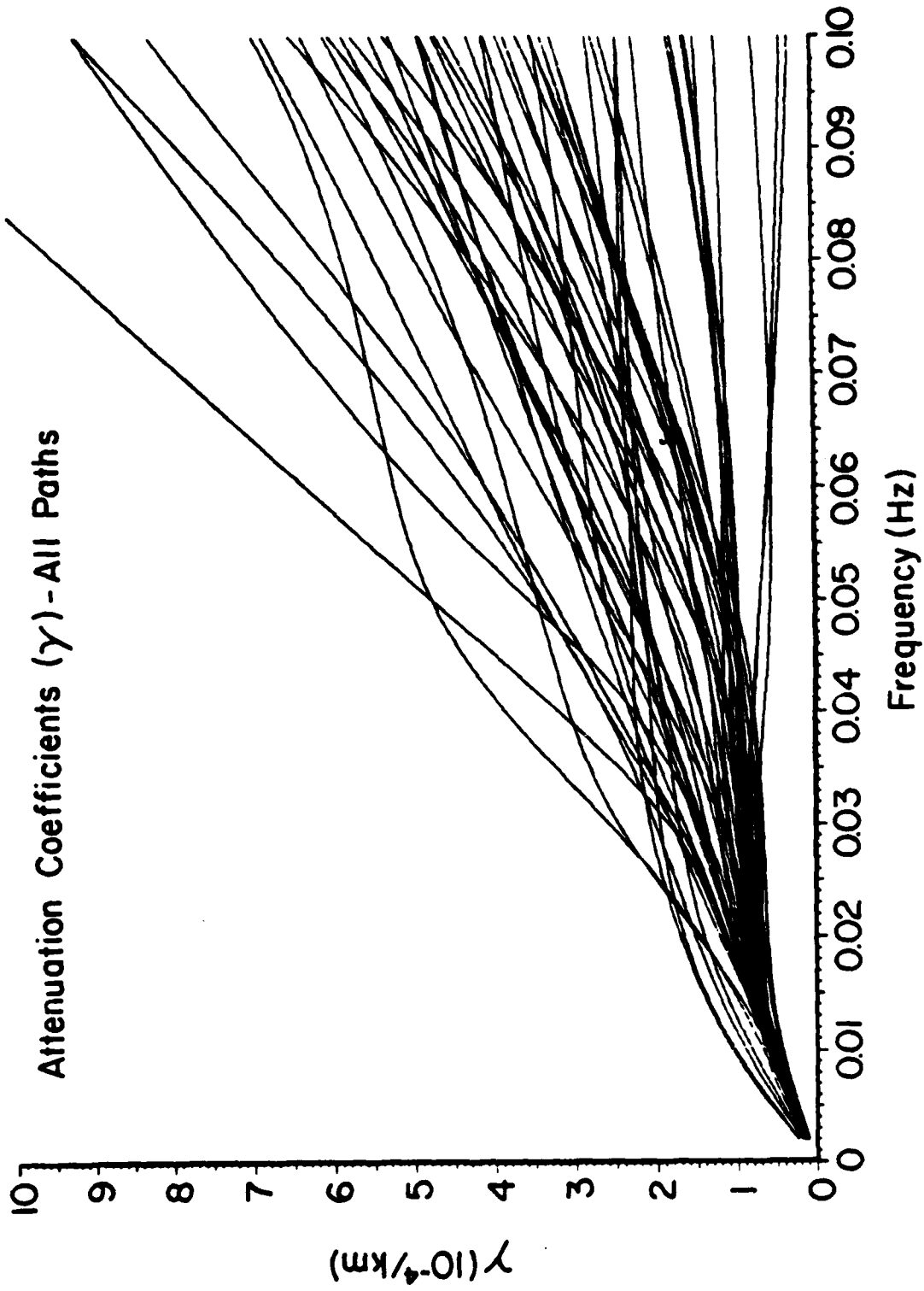


Figure 20. Attenuation coefficients for all paths from NTS and East Kazakh.

TABLE 4
 AVERAGE 20 SECOND VALUES FOR NTS AND
 EAST KAZAKH PATHS (MKS UNITS)

Paths	Phase Velocity $C(x10^3)$	Group Velocity $U(x10^3)$	Ellipticity ϵ	Excitation Function $S_1(x10^{-14})$	Path Amplitude Function $S_2(x10^{-5})$	Attenuation Coefficient $\gamma(x10^{-7})$
All	3.52 ± 0.14	3.00 ± 0.17	-0.72 ± 0.64	3.87 ± 0.64	8.65 ± 0.46	1.97 ± 1.02
East Kazakh	3.45 ± 0.13	2.95 ± 0.14	-0.71 ± 0.03	4.08 ± 0.67	8.80 ± 0.44	2.12 ± 1.21
NTS	3.54 ± 0.13	-0.02 ± 0.18	-0.72 ± 0.04	3.80 ± 0.62	8.61 ± 0.46	1.87 ± 0.91
NTS-WWSSN	3.48 ± 0.05	2.95 ± 0.06	-0.74 ± 0.04	4.11 ± 0.38	8.72 ± 0.19	1.89 ± 0.97
NTS-SR0	3.66 ± 0.16	3.16 ± 0.25	-0.68 ± 0.02	3.20 ± 0.56	8.37 ± 0.72	1.82 ± 0.80
Oceanic	3.89 ± 0.08	3.50 ± 0.09	-0.68 ± 0.02	2.43 ± 0.17	7.50 ± 0.22	1.52 ± 0.66

IX. ESTIMATED MOMENTS FOR NTS AND EAST KAZAKH EXPLOSIONS

We have estimated explosion moments for the 40 NTS explosions and 18 East Kazakh explosions which were recorded at two or more stations. The estimated moments (in MKS units, newton-meters), together with their network standard deviations and the number of stations used in the average are given in Tables 5 and 6. The yields given in Table 5 are from Marshall, et al. (1979). The network standard deviations in (log) moment are quite small, about 0.1. Even for recent NTS explosions, which include data from several distant SR0 stations, the standard deviations are only about 0.15.

As a check on the results, we calculated residual station corrections for all paths. These are listed in Tables 7 and 8. These station corrections are designed to minimize the variance in moment over the network at stations observing each event. Most of the station corrections are small, particularly for shorter paths. Eighteen of the 24 WWSSN stations have station residuals of 0.1 or less. The station corrections increase with distance from the source, which is to be expected because of the increasing complexity of the travel paths, but the largest corrections for some very complex paths are only about 0.3.

Sykes and Cifuentes (1984) measured M_s values for a similar set of East Kazakh explosions. Our moment estimates are very consistent with their reported M_s values. Using the ten normal events that the two data sets have in common we find the following moment/ M_s relation:

$$\log M_0 = M_s + 11.86 \pm 0.03$$

where the ± 0.03 is the standard deviation over all ten events.

It is interesting to compare the results for recent events with theoretical explosion models. Since April 1976, underground explosions have been limited to a yield of 150 kilotons by the Threshold Test Ban Treaty. In Figure 21, we show the estimated

TABLE 5
NTS EXPLOSIONS

Event	Date	Area*	Number of Stations	Log Moment	Standard Deviation	Remarks
Corduroy	12/03/65	Y	5	16.10	0.14	
Dumont	05/19/66	Y	5	15.98	0.13	
Piledriver	06/02/66	C	6	15.84	0.12	Yield 62 KT, Reversed
Commodore	05/20/67	Y	5	16.27	0.26	Yield 250 KT
Scotch	05/23/67	P	7	16.46	0.18	Yield 155 KT
Zaza	09/27/67	Y	6	16.32	0.14	
Lanpher	10/18/67	Y	4	15.87	0.06	
Stinger	03/22/68	P	3	16.17	0.09	
Sled	08/29/68	P	10	16.22	0.09	
Noggin	09/06/68	Y	6	16.05	0.06	
Purse	05/07/69	P	9	16.42	0.06	
Tijeras	10/14/70	Y	5	16.01	0.13	
Oscuro	09/21/72	Y	3	15.99	0.11	
Almendro	06/06/73	P	10	16.78	0.11	
Escabosa	07/10/74	Y	7	16.14	0.15	
Portmanteau	08/30/74	Y	2	16.08	0.00	
Topgallant	02/28/75	Y	2	15.83	0.09	
Tybo	05/14/75	P	10	16.50	0.10	
Stilton	06/03/75	P	5	16.17	0.12	
Mizzen	06/03/75	Y	5	16.02	0.15	
Mast	06/19/75	P	12	16.58	0.15	
Cheshire	02/14/76	P	4	16.79	0.39	
Estuary	03/09/76	P	4	16.79	0.05	
Pool	03/17/76	P	3	16.52	0.09	
Strait	03/17/76	Y	3	16.28	0.15	
Marsilly	04/05/77	Y	2	16.01	0.06	150 KT Limit Begins
Sandreef	11/09/77	Y	15	16.27	0.15	
Farallones	12/14/77	Y	2	16.22	0.02	
Iceburg	03/23/78	Y	2	16.15	0.07	
Lowball	07/12/78	Y	4	15.96	0.07	
Panir	08/31/78	P	8	15.97	0.15	
Rummy	09/27/78	Y	16	16.12	0.15	
Farm	12/16/78	P	7	15.89	0.18	
Pepato	06/11/79	P	17	16.07	0.13	
Hearts	09/06/79	Y	16	16.12	0.15	
Sheepshead	09/26/79	P	14	15.95	0.14	
Pyramid	04/16/80	Y	5	15.65	0.08	
Colwick	04/26/80	P	7	15.91	0.18	
Kash	06/12/80	P	8	16.16	0.09	
Tafi	07/25/80	P	7	16.10	0.09	

*Y = Yucca Flat, P = Pahute Mesa, C = Climax Stock

TABLE 6
EAST KAZAKH EXPLOSIONS

Date	Number of Stations	Log Moment	Standard Deviation	Remarks
07/04/76	3	15.73	0.18	
06/11/78	5	15.94	0.04	
09/15/78	6	15.74	0.10	
11/29/78	9	15.75	0.11	
06/23/79	10	15.83	0.09	
08/04/79	10	15.94	0.12	
08/18/79	9	15.69	0.20	Reversed
10/28/79	6	15.85	0.08	
12/02/79	9	15.96	0.11	
12/23/79	3	15.66	0.20	Large body waves
09/14/80	10	15.86	0.09	Reversed
10/12/80	7	15.94	0.09	
04/22/81	7	15.92	0.09	
09/13/81	4	15.87	0.32	Very low at KAA0
10/18/81	3	15.91	0.13	
12/27/81	5	15.92	0.09	
04/25/82	5	15.85	0.10	
12/05/82	5	15.92	0.12	

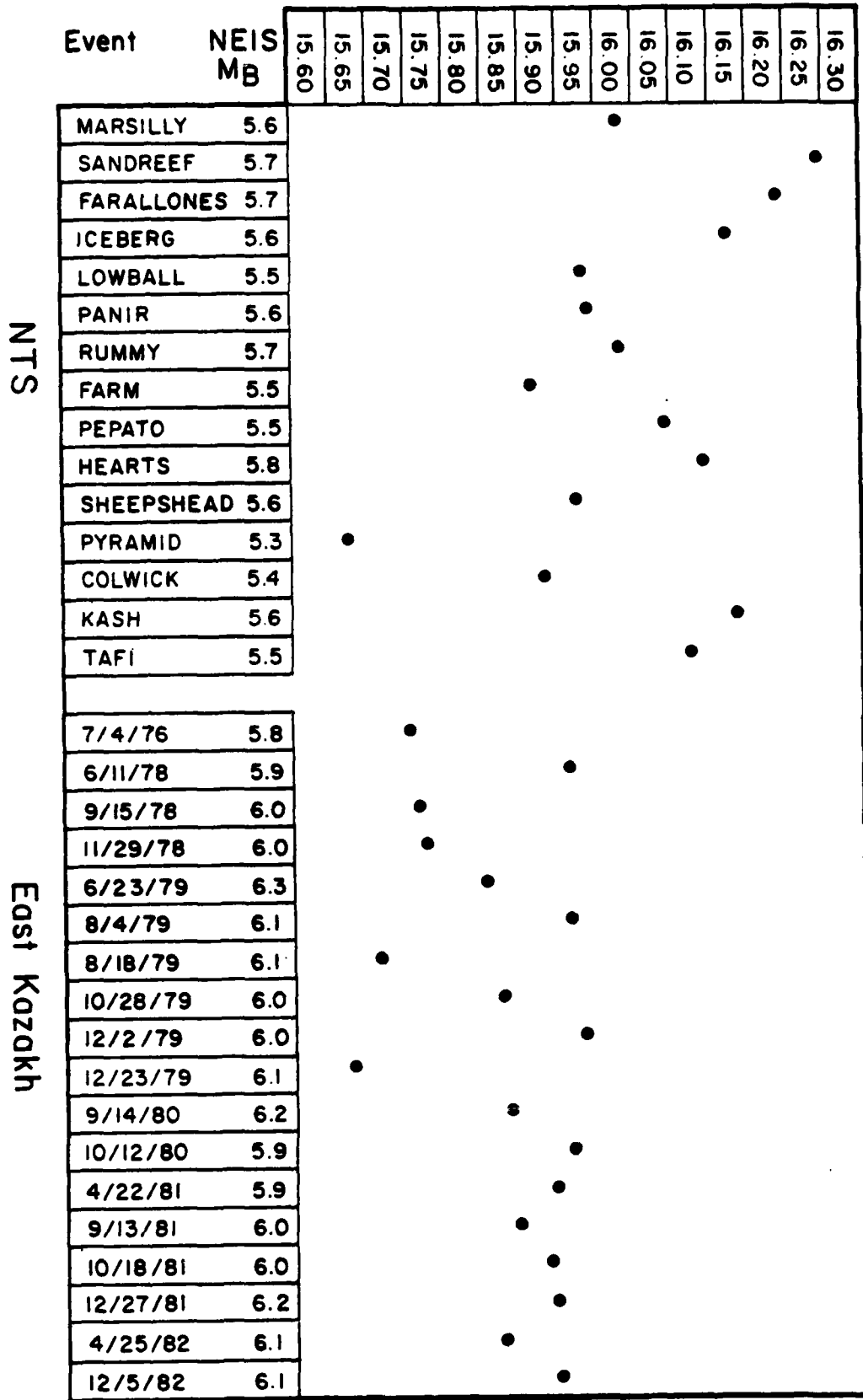
TABLE 7
NTS SURFACE WAVE PATHS

Station	Average Distance (km)	Number of Events	Residual Station Correction
AAM	2830	8	0.07
ALQ	907	10	-0.06
BLA	3169	10	-0.07
BLC	3305	5	0.05
COL	3703	10	-0.12
COR	1006	10	-0.01
DAL	1843	6	-0.06
FCC	2885	3	0.10
FSJ	2018	4	0.18
GOL	982	26	-0.02
JCT	1684	13	-0.15
LHC	2517	4	-0.16
LON	1156	13	0.07
LUB	1358	16	-0.01
MBC	4359	8	-0.12
OGD	3586	8	0.12
OTT	3475	13	-0.02
OXF	2445	4	0.06
RES	4330	7	-0.04
SCP	3324	16	-0.07
SES	1522	6	0.26
SHA	2680	8	-0.05
VIC	1372	3	-0.06
WES	3859	5	0.04
ANTO	10910	5	0.32
BCAO	7545	4	0.00
BOCO	5625	4	-0.22
CHTO	12830	2	-0.33
CTAO	11990	7	0.08
GRFO	9098	4	0.13
KAAO	12080	6	0.12
KONO	8191	6	0.27
MAIO	11880	3	-0.01
MAJO	8804	5	0.17
TATO	10890	4	-0.18
ZOBO	7746	10	-0.05

TABLE 8
EAST KAZAKH SURFACE WAVE PATHS

Station	Average Distance (km)	Number of Events	Residual Station Correction
ANMO	10610	14	-0.01
ANTO	3742	10	0.00
BCAO	7545	6	-0.02
CHTO	3888	10	0.08
GRFO	4706	13	-0.16
GUMO	7144	15	-0.04
KAAD	1888	9	0.10
KONO	4377	15	0.10
MAIO	2173	6	0.11
MAJO	4905	14	-0.06
SHIO	2926	4	0.07
ZOBO	15250	4	-0.09

Log Moment (Newton-Meters)



Estimated Moments - Explosions Since 1976

Figure 21. Estimated moments for the largest NTS and East Kazakh explosions since April 1976.

moments for the largest explosions at NTS and East Kazakh since this date. Using a Mueller-Murphy explosion model (Mueller and Murphy, 1971), the log moment of a 150 kiloton explosion in a tuff/rhyolite medium should be 16.24. This agrees very well with the upper limit of the recent NTS explosion estimated moments.

A surprising result is the low values of moment estimated for the East Kazakh explosions. None of the explosions has an estimated log moment greater than 16.0. The upper limit of the log moments for East Kazakh is about 0.2 less than the upper limit of log moments for NTS. This contrasts dramatically with the NEIS m_b values for the explosions (also shown in Figure 21). Several of the East Kazakh explosions have m_b greater than 6.1, while none of the NTS explosions has an m_b greater than 5.8. Comparison with theoretical explosion models makes the contrast even larger. It is commonly believed that the source medium at the East Kazakh test site is a hard "granite-like" material (e.g., Alewine and Bache, 1983), but the log moment for a 150 kiloton Mueller-Murphy explosion in granite is 16.52, more than 0.5 greater than the largest estimated moment at East Kazakh. Furthermore, the difference between m_b and M_s due to local elastic properties at the source should be larger for a low velocity material than for a high velocity material (Stevens and Day, 1985).

Several factors, including tectonic strain release, differences in body wave attenuation, or an unusual source medium could account for these differences. Correction for tectonic strain release could increase the moments of some events to the level of the largest NTS explosions (Stevens, 1982; Sykes and Cifuentes, 1984), but could not increase them to the level expected for a 150 kiloton granite source. The East Kazakh explosions are therefore not consistent with a "granite-like" source medium. One possible explanation for the large body waves and small surface waves from East Kazakh explosions would be the presence of a source medium at the test site that resulted in a highly peaked source spectrum with a large amplitude near one Hz and an unusually small long period level.

X. THE EFFECT OF SOURCE REGION STRUCTURE ON MOMENT ESTIMATES

It is important to assess the consequences of the constraints and assumptions that were used in making our moment estimates. The two most important constraints were the model for the elastic structure of each source region and the constraint placed on the upper mantle Q . In this section and the following section, we examine the variations in moment estimates that result from changes in these assumptions.

The East Kazakh source region structure is based on the best available information about the region, but this information cannot be regarded as definitive so we want to estimate the maximum reasonable error in our excitation function for this region. In Figure 22, we show the excitation functions S_1 calculated from all of the earth structures that we have found by surface wave inversion. There is a substantial amount of variation in the excitation functions with a total variation of about a factor of two. The smallest excitation functions, however, belong to oceanic and mixed paths, and the largest are for thick crust, low velocity paths to the southeast of East Kazakh. In Figure 23 we show the excitation functions for all of the continental paths out of East Kazakh. The variation in S_1 is reduced substantially. The lowest amplitude excitation function belongs to the high velocity shield path from East Kazakh to station KONO.

To estimate the uncertainty in the excitation function, we used the East Kazakh to KONO structure, with the surface velocities modified to be the same as in the structure used for our Q /moment inversions described earlier. We calculated the excitation function for this structure and inverted the spectra for all paths out of East Kazakh to obtain new moment estimates. The log moments were increased by 0.04 on the average.

Source Region Excitation Function (S1) - All Paths

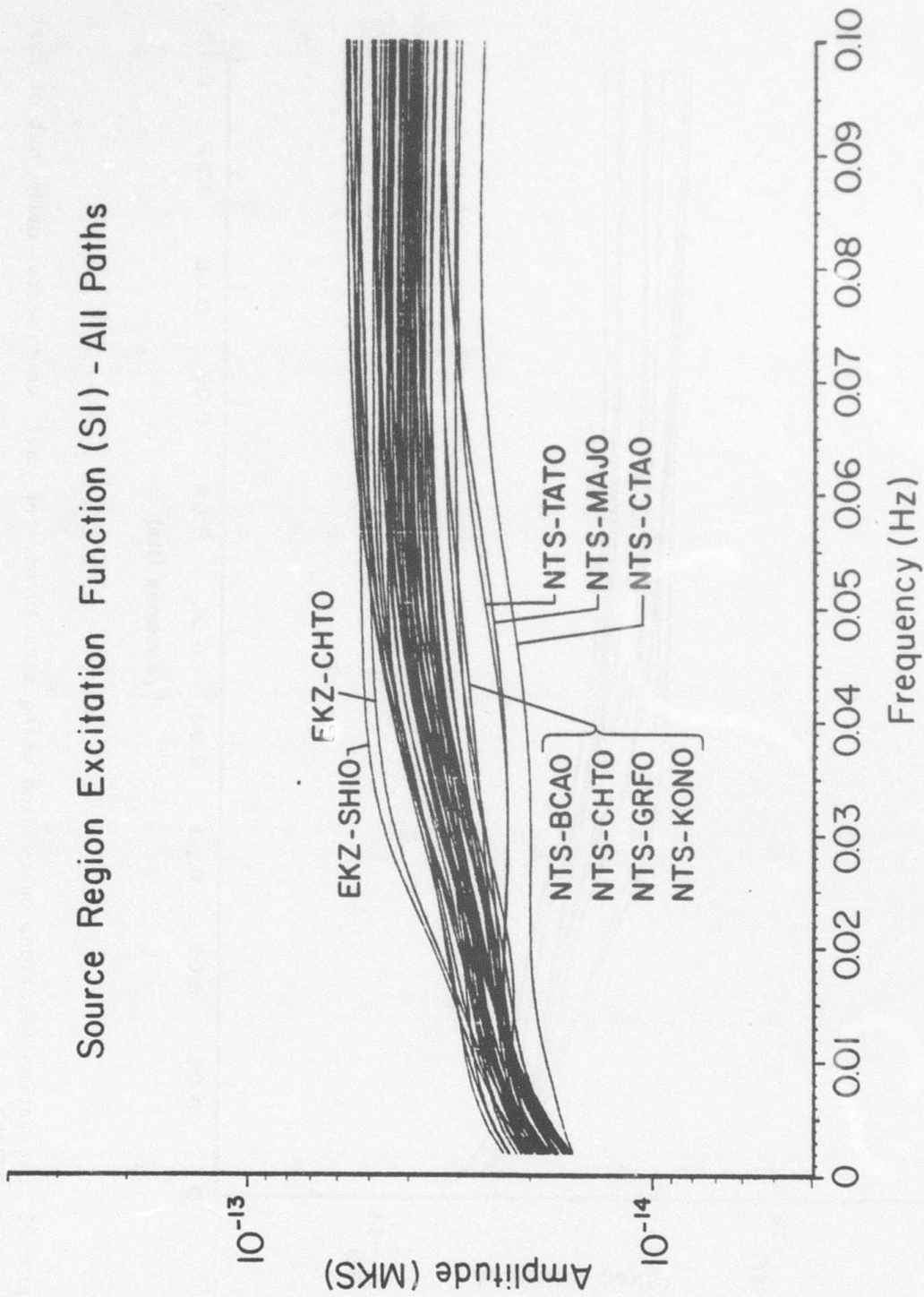


Figure 22. Excitation function S_1 calculated using the structures found for all paths from NTS and East Kazakh.

S1 for Continental Paths from East Kazakh

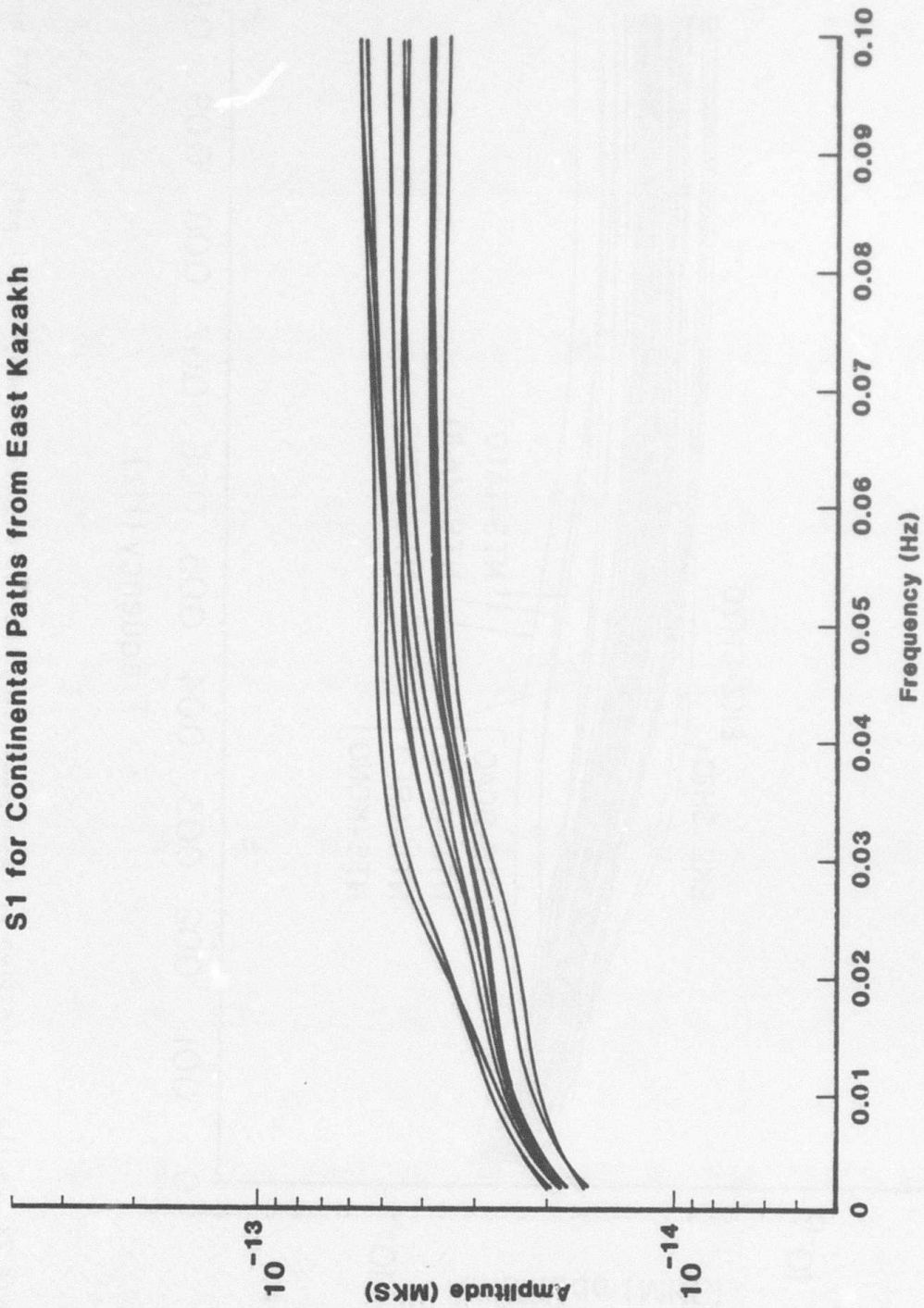


Figure 23. Excitation functions calculated using structures for all continental paths out of East Kazakh.

The most important feature of the NTS source region structure is the shallow shear velocity. In Figure 24 we show the variation of the source region excitation function S_1 calculated at a frequency of 0.05 Hz as a function of the shear velocity at the source depth of one kilometer. In these calculations, the shear velocity in the upper 1.5 kilometers of the NTS source region model was varied, the compressional velocity was set using a constant Poisson's ratio of 0.27 and the density in this layer was held fixed. The phase and group velocities at this low frequency depend only weakly on the shear velocity, but the excitation function S_1 is quite sensitive to the shallow velocity structure, varying approximately as $S_1 \sim \beta^{-0.7}$.

The shear velocity at the source depth used in the earlier moment estimates for NTS was 2.0 km/sec. Bache, *et al.* (1975) give shear velocities in tuff and rhyolite at NTS ranging from 1.5 to 2.5 km/sec, so this is a good average value for the shear velocity at NTS. The lowest hard rock velocities at NTS are found in dry tuff, which have shear velocities of about 1.0 km/sec. To put an upper bound on the NTS source region excitation function, we modified the NTS model to have a shear velocity in the upper 1.5 km of 1.0 km/sec, calculated the excitation function for this structure, and reinverted all of the spectra for NTS paths to obtain new moment estimates. Log moment estimates were reduced by 0.08 on the average.

The excitation functions for NTS and East Kazakh are shown in Figure 25 together with the excitation functions calculated from the two perturbed structures described here. The excitation functions are very frequency dependent, so it is not possible to tell at a glance what the effect of the excitation function is on the moment estimates. To estimate the effect of the different source regions used for NTS and East Kazakh, we reinverted the spectra for East Kazakh paths using the NTS source region model. The log moments were decreased on the average by 0.02.

20 Second Sensitivity to Shallow Shear Velocity

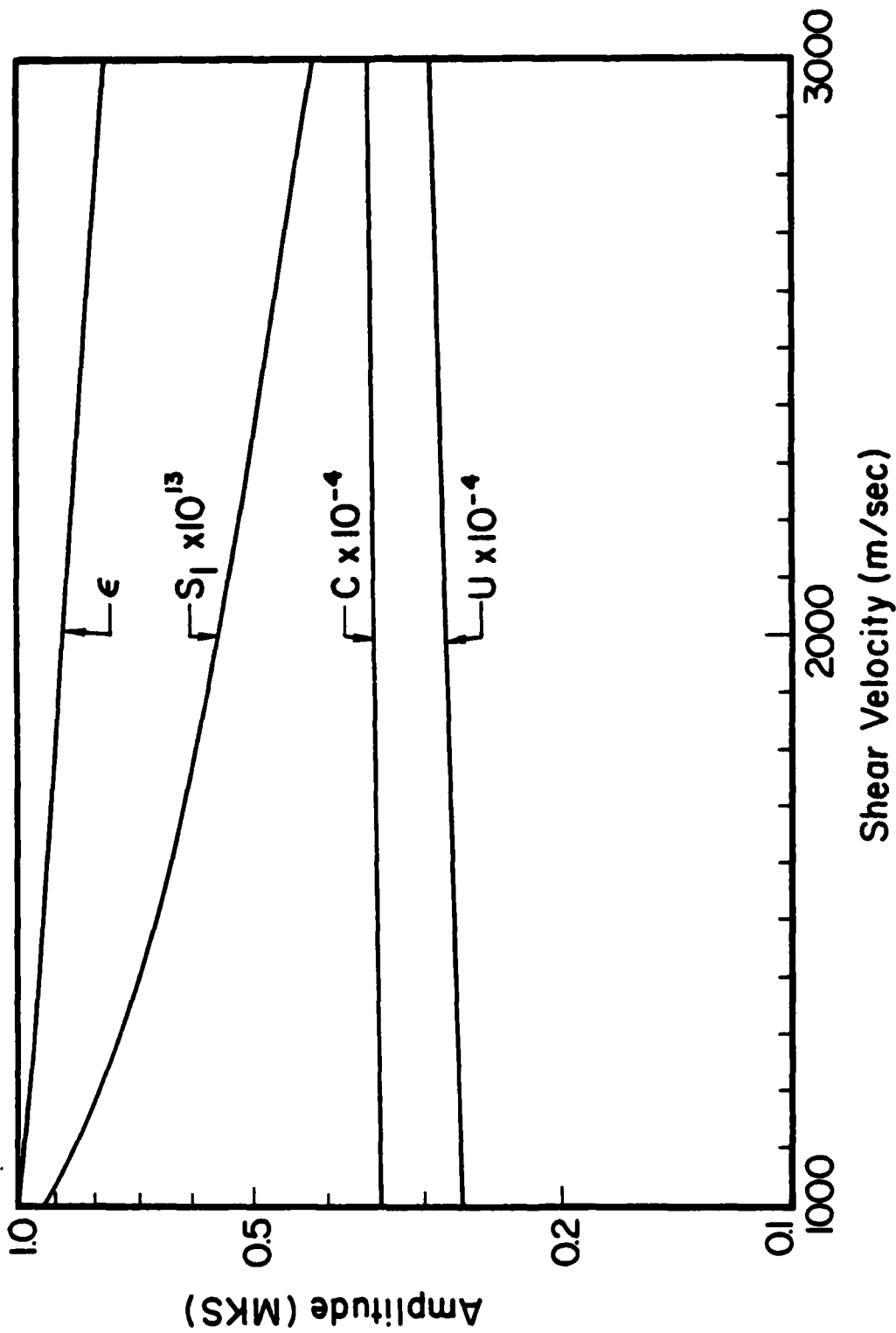


Figure 24. The dependence of the 20 second excitation function S_1 , ellipticity ϵ , phase velocity c , and group velocity U on the shallow shear velocity structure. Calculations were made using the NTS structure in Figure 17 and varying the velocity in the upper 1.5 km. The 20 second excitation function is strongly affected by the shallow structure.

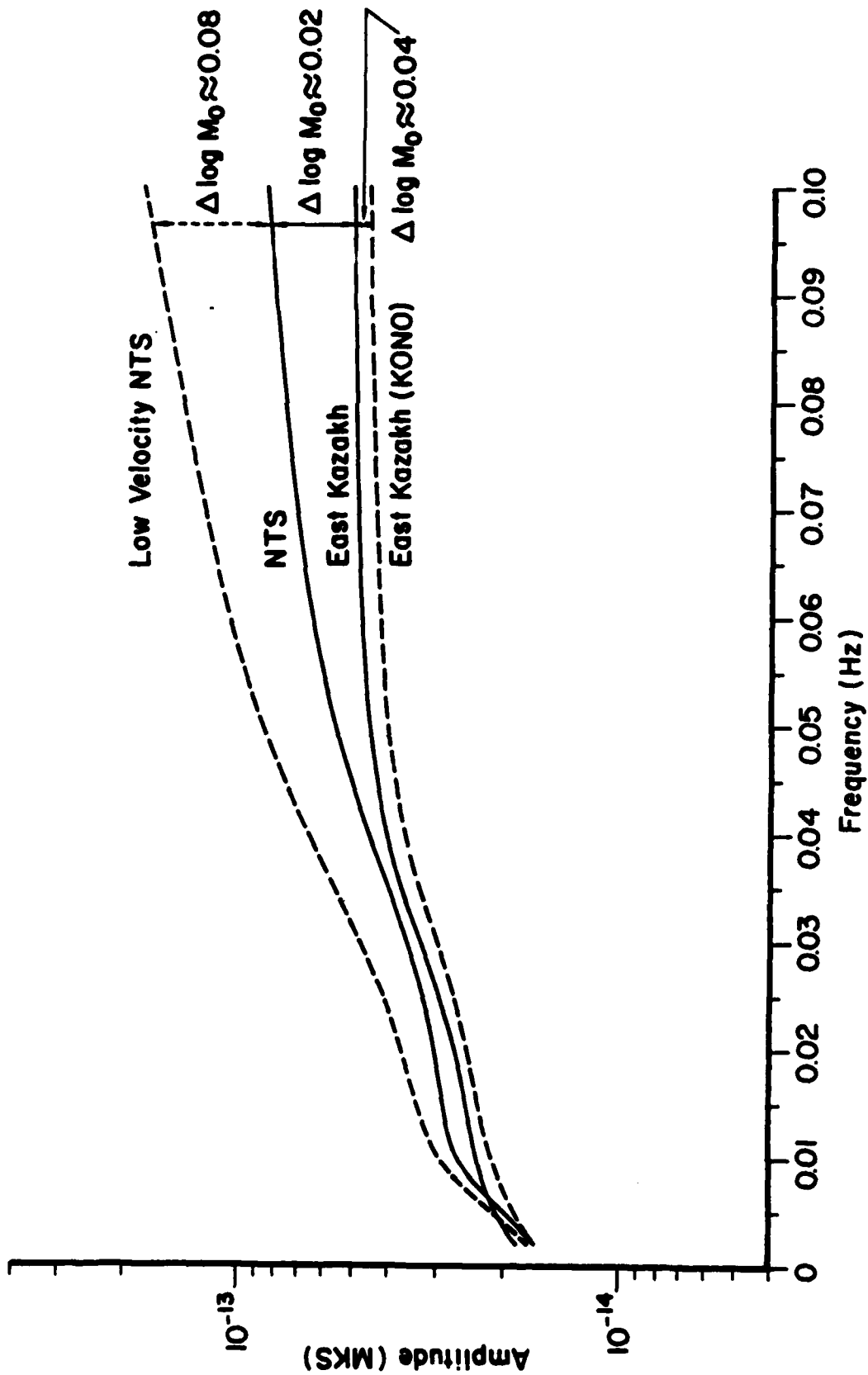


Figure 25. Excitation functions calculated from NTS and East Kazakh source region structures. The lower dashed line is the excitation function derived from the East Kazakh to KONO path structure. The upper dashed line is the excitation function for the NTS structure with the shear velocity at the source depth reduced to 1.0 km/sec. Estimates for $\Delta \log m_b$ were obtained by inverting spectra from NTS and East Kazakh paths for Q and moment using each excitation function.

Correction for source region structure reduces estimated moments for NTS explosions by approximately 0.02 relative to estimated moments for East Kazakh explosions. This correction would be larger if either the NTS near surface velocities were lower than the values used, or if the East Kazakh crustal velocities were higher than those used in the model. Note also that the correction to the spectral amplitudes increases with frequency. The correction to a 20 second spectral magnitude should be approximately 0.09. The correction to moment is smaller because the moment estimate depends more strongly on long period amplitudes than on short period amplitudes, and because there is a tradeoff between the source region correction and the attenuation correction. For a given observed Rayleigh wave spectrum, moment estimation using the NTS structure will result in a larger attenuation correction than moment estimation using the East Kazakh structure, since the inversion will assume (properly) that if the observed spectrum had contained the amount of high frequency energy shown in the NTS excitation function in Figure 25 at the source, it must have been attenuated by the time it reached the receiver.

One final point should be made about the source region correction. In Section II, we defined S_1 so that we find the normalized moment M'_0 rather than the moment M_0 . This choice is appropriate since M'_0 is a representation of the source of the surface waves that is independent of local material properties, and since there is no evidence that M_0 correlates with yield better than M'_0 . We can, of course, convert M'_0 to M_0 if local velocities are known through the relation

$$M_0 = \frac{a^2}{3\beta^2} M'_0$$

Since Poisson's ratio is probably lower at East Kazakh than at NTS (because of stronger, more competent rock), this conversion would increase estimated moments at NTS relative to estimated moments at East Kazakh.

XI. THE EFFECT OF MANTLE Q CONSTRAINTS ON MOMENT ESTIMATES

A good check on the validity of the mantle Q constraint is the variation of the moment estimates as a function of distance. In Figure 26, we show the station residuals for all NTS and East Kazakh paths plotted versus distance. The station residuals are small at close range, approximately 0.1 for most stations less than 5000 kilometers from a test site. The magnitude of the residuals increases with distance, as is to be expected with the increasing complexity of the path at large distances, but the residuals scatter evenly around zero. The lack of any trend in the data suggests that the attenuation correction has been properly estimated with the constraint of $\beta/Q = 40$ between 120 and 150 kilometers depth.

In Figures 27, 28, and 29 we show station residuals with constraints of $\beta/Q = 25$, 50 and 100 respectively. With the lower attenuation of $\beta/Q = 25$ ($Q \sim 180$), the station residuals clearly increase with distance indicating that the moments are undercorrected for attenuation. The relative moments at the two test sites are not changed significantly, however. The log moments are decreased by 0.05 at NTS and by 0.07 at East Kazakh. Increasing attenuation slightly with $\beta/Q = 50$ ($Q \sim 90$), the station residuals show little trend with distance and the moments are increased by 0.03 at East Kazakh and by 0.04 at NTS. If attenuation is increased to $\beta/Q = 100$ ($Q \sim 45$), then the station residuals show a strongly decreasing trend with distance indicating that the moments have been overcorrected for attenuation. In this case the moments are increased by 0.22 at NTS and by 0.23 at East Kazakh.

Based on these tests, we conclude that a constraint of $\beta/Q \approx 40-50$ in the upper mantle is appropriate. The relative moments between the two test sites is insensitive to the choice of constraint as long as the same constraint is used for both test sites and the distribution of stations is comparable for both test sites.

Station Residual Beta/Q = 40

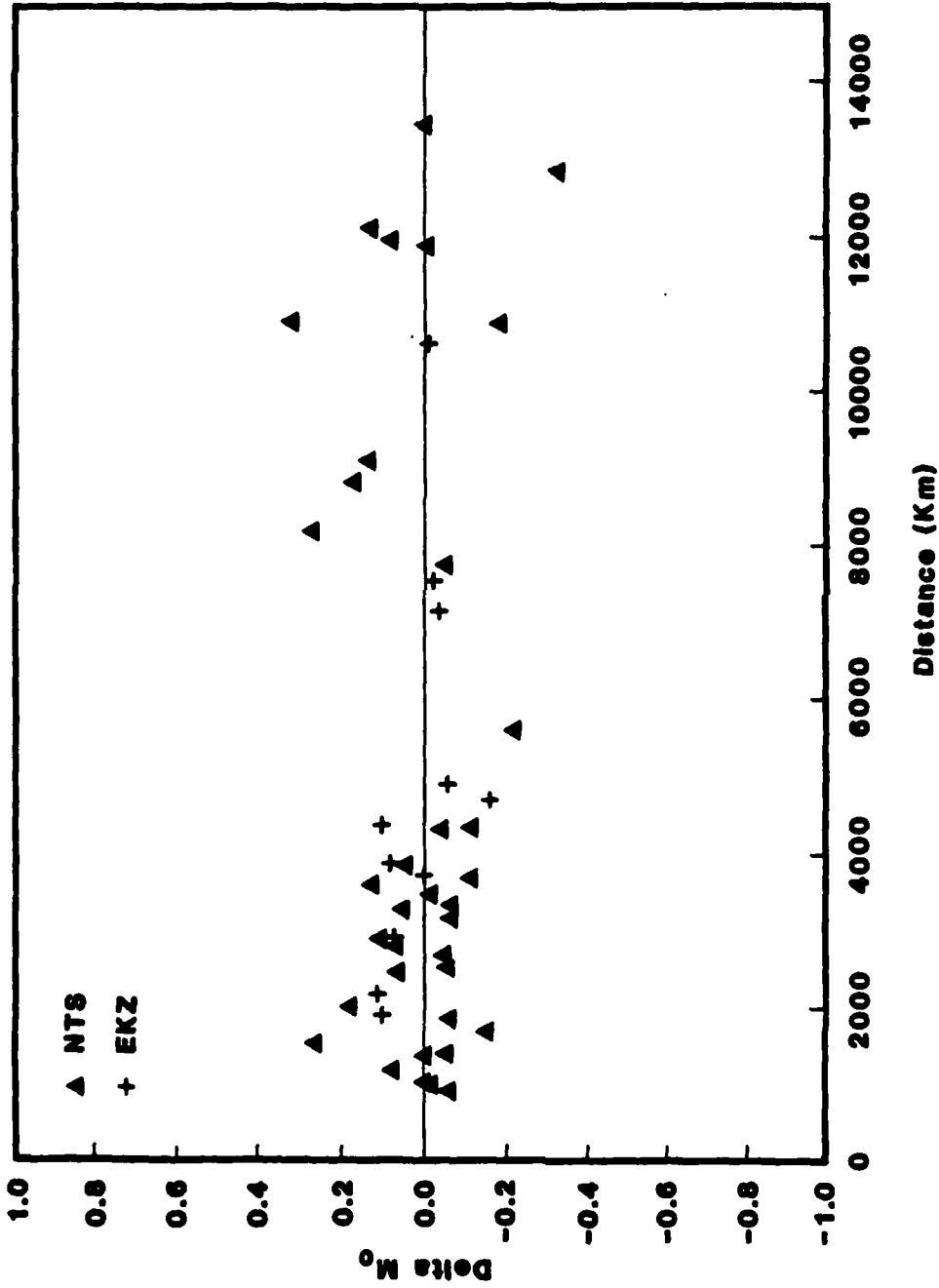


Figure 26. Station residuals with a mantle Q constraint of $\beta/Q = 40$.

Station Residual Beta/Q = 25

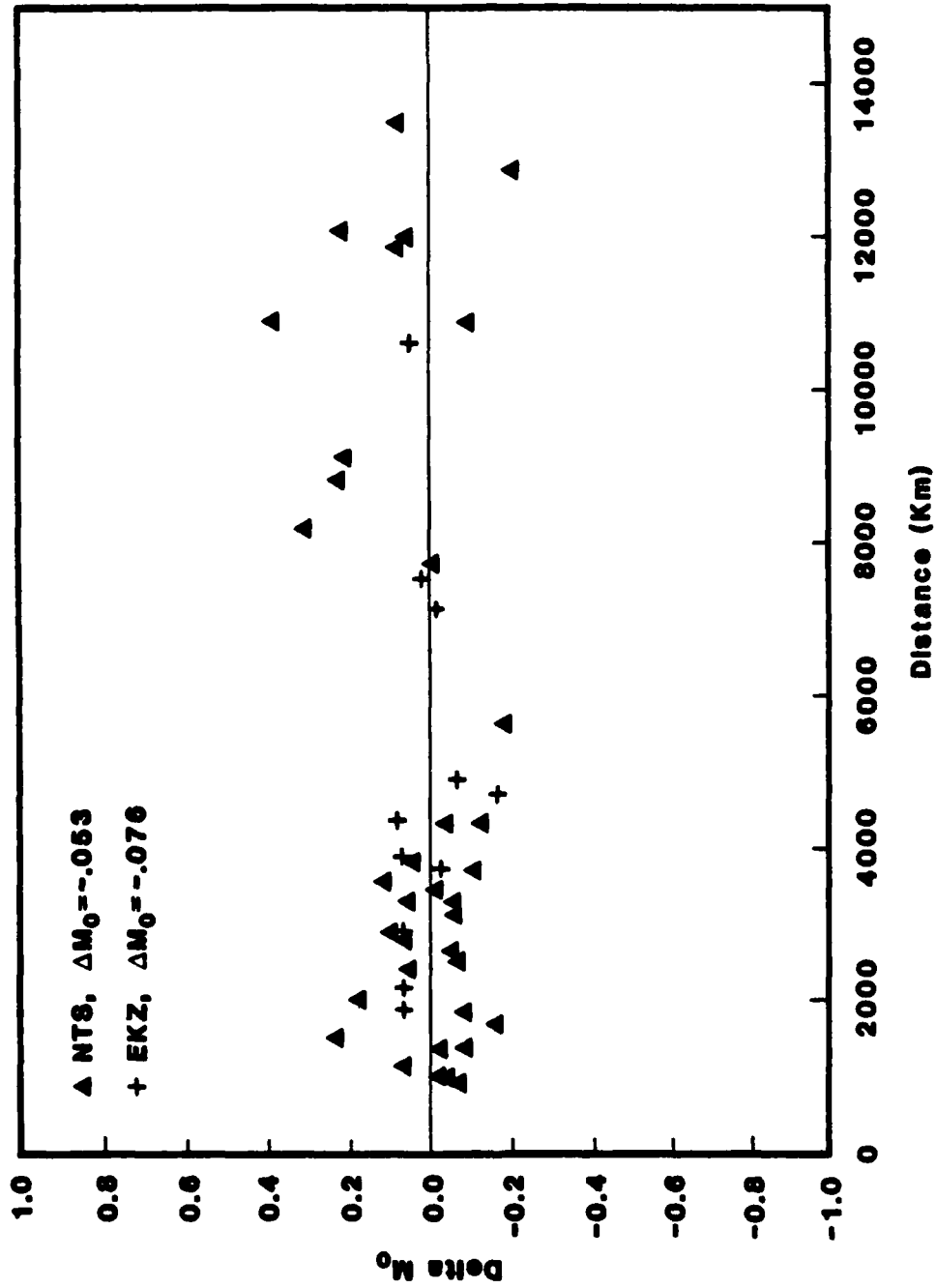


Figure 27. Station residuals with mantle Q constraint of $\beta/Q = 25$.

The value of β/Q in the mantle is not, of course, constant throughout the earth. Because of the finite frequency range of the data, we cannot directly determine the mantle Q , and our approach has been to use an average value as a constraint and to accept some scatter in the results, rather than to try to make uncertain corrections for variations in mantle Q . This is particularly appropriate for long paths, where the Q correction is most important, since many different regions of the earth are sampled by the Rayleigh wave between the source and receiver.

An interesting question is the effect of a small region of the travel path with a mantle Q significantly different from the average value. As we mentioned earlier, for example, interstation Q studies have found much lower mantle Q values near NTS (e.g., Lee and Solomon, 1979) than near East Kazakh (e.g., Patton, 1980). If the mantle Q is lower than our average value, then the attenuation coefficients will be underestimated. From Equation (6), we find for a moment estimate M_0 made from an observed spectrum $u(\omega)$,

$$\Delta \ln M_0 = \Delta(r\gamma(\omega)) \quad (9)$$

so if γ is underestimated, M_0 will also be underestimated by an amount that depends on the length of the travel path with the different Q value. Comparing results from our test cases above, we find that changing mantle β/Q from 40 to 25 decreases γ by approximately $0.3 \times 10^{-4}/\text{km}$ over the frequency range 0.02 to 0.05 Hz. Changing β/Q from 40 to 100 increases γ by approximately $1.0 \times 10^{-4}/\text{km}$ over the same frequency range. If $\beta/Q = 100$ were a better value for mantle Q for a region approximately 1000 km around NTS, then our $\log M_0$ estimates for NTS explosions would be low by about 0.04. If $\beta/Q = 25$ were a better value for mantle Q for a region 1000 km around East Kazakh, then our $\log M_0$ estimates would be high by approximately 0.01. Making this additional correction would therefore increase the NTS moments relative to the East Kazakh moments by approximately 0.05.

SUMMARY AND CONCLUSIONS

In summary, the most important conclusions of this report are:

- * The path correction procedure does provide stable and accurate measurements of surface waves.
- * Typical network scatter in log moment is about 0.1 compared to 0.2 or more for network scatter in M_s .
- * Dispersion is not a problem since this is a spectral method. Data from stations at close range (less than 30 degrees) can be used without difficulty.
- * The spectrum is flattened by application of the path correction, so the results are nearly frequency independent. Moments are estimated from an average over a range of frequencies.
- * Little variability in spectral amplitudes results from the elastic structure of the travel path.
 - * The standard deviation on the logarithm of the path amplitude function over all of the paths processed is only 0.025. The extreme values differ by only 0.15.
 - * This result contrasts dramatically with time domain amplitudes which have large variations due to path dependent dispersion.
- * The elastic structure of the source region can significantly affect surface wave amplitudes.
 - * Assuming that the surface velocities are higher at East Kazakh than at NTS, surface wave amplitudes should be larger for NTS explosions than for East Kazakh explosions with the same moment.

- * Correction for source region structure based on the best models available for the two test sites reduces the estimated log moment of NTS explosions by 0.02 relative to log moments for explosions at the East Kazakh test site.
- * Attenuation differences can cause large variations in surface wave amplitudes at distant stations. An important check on the attenuation correction is the variation of moment estimates with distance.
 - * When the Q inversion is performed with the mantle Q constrained to a value of approximately 100 at depths of 120 to 150 kilometers, the moment estimates remain constant (on the average) with distance.
 - * When the Q inversion is performed with a Q constraint a factor of two higher or lower, the moment estimates show a significant trend with distance indicating under or overcorrection for attenuation.
 - * The relative moments between the two test sites are insensitive to changes in the Q constraint.

XIII. REFERENCES

- Alewine, R. W. and T. C. Bache (1983), "Monitoring a Threshold Test Ban Treaty, EOS Trans. Am. Geophys. Un., 64, 193.
- Anderson, D. L., A. Ben Menahem and C. B. Archambeau (1965), "Attenuation of Seismic Energy in the Upper Mantle," JGR, 70, 1441-1448.
- Anderson, D. L. and R. S. Hart (1976), "An Earth Model Based on Free Oscillations and Body Waves," JGR, 81, 1461-1475.
- Anderson, D. L. and R. S. Hart (1978), "Q of the Earth," JGR, 83, 5869-5882.
- Archambeau, C. B., E. A. Flinn and D. G. Lambert (1966), "Detection, Analysis, and Interpretation of Teleseismic Signals, 1, Compressional Phases from the SALMON Event," JGR, 71, 3483-3501.
- Bache, T. C., T. R. Blake, J. T. Cherry, T. G. Barker, D. G. Lambert, J. M. Savino and N. Rimer (1975), "An Explanation of the Relative Amplitudes of the Teleseismic Body Waves Generated by Explosions in Different Test Areas at NTS," Systems, Science and Software Final Report DNA 3958F (SSS-R-76-2746), submitted to DNA, October.
- Bache, T. C., W. L. Rodi and D. G. Harkrider (1978a), "Crustal Structures Inferred from Rayleigh Wave Signatures of NTS Explosions," BSSA, 68, No. 5, 1399-1413.
- Bache, T. C., W. L. Rodi and B. F. Mason (1978b), "Source Amplitudes of NTS Explosions Inferred from Rayleigh Waves at Albuquerque and Tucson," Systems, Science and Software Topical Report submitted to DARPA, SSS-R-78-3690, June.
- Beliaevsky, N. A., A. A. Borisov, I. S. Volvovsky and Y. K. Schukin (1968), "Transcontinental Crustal Sections of the U.S.S.R. and Adjacent Areas," Canadian Journal of Earth Sciences, 5, 1067-1078.
- Canas, J. A. and B. J. Mitchell (1978), "Lateral Variation of Surface-Wave Anelastic Attenuation Across the Pacific," BSSA, 68, 1637-1650.
- Canas, J. A. and B. J. Mitchell (1981), "Rayleigh Wave Attenuation and Its Variation Across the Atlantic Ocean," Geophys. J. R. Astr. Soc., 67, 159-176.

- Cara, M. (1981), "Differential Attenuation Coefficients for Rayleigh Waves: A New Constraint on Q-Models," in Anelasticity in the Earth, Geodynamics Series, Vol. 4, American Geophysical Union.
- Dobrin, M. B. (1976), "Introduction to Geophysical Prospecting, McGraw Hill, New York.
- Dziewonski, A. M., J. Bloch and M. Landisman (1969), "A Technique for the Analysis of Transient Seismic Signals," BSSA, 59, 427-444.
- Glover, P. and D. Harkrider (1981), "Evaluation of Mixed Path Rayleigh Techniques Using the Representation Theorem," EOS Trans. Am. Geophys. Union, 62, 947.
- Grand, S., D. V. HelMBERGER and L. J. Burdick (1984), "An Attenuation Bias Measurement for the Semipalatinsk Test Site from Multiple S Phases," Woodward-Clyde Semiannual Technical Report submitted to DARPA, WCCP-R-84-06, August.
- Harkrider, D. G. (1964), "Surface Waves in Multilayered Media I. Rayleigh and Love Waves from Buried Sources in a Multilayered Elastic Half Space," BSSA, 54, 627-629.
- Harkrider, D. G. (1970), "Surface Waves in Multilayered Media II. Higher Mode Spectra and Spectral Ratios from Point Sources in Plane-Layered Earth Models," BSSA, 60, 1937-1987.
- Herrin, E. and T. Goforth (1977), "Phase-Matched Filtering: Application to the Study of Rayleigh Waves," BSSA, 67, 1259-1275.
- Lee, W. B. and S. C. Solomon (1979), "Simultaneous Inversion of Surface Wave Phase Velocity and Attenuation: Rayleigh and Love Waves over Continental and Oceanic paths," BSSA, 69, 65-95.
- Marshall, P. D., D. L. Springer and H. C. Rodean (1979), "Magnitude Corrections for Attenuation in the Upper Mantle," Geophys. J. R. Astr. Soc., 57, 609-638.
- McEvelly, T. (1964), "Central U. S. Crust-Upper Mantle Structure from Love- and Rayleigh-Wave Phase Velocity Inversion," BSSA, 54, 1992-2015.
- Mitchell, B. J. (1975), "Regional Rayleigh Wave Attenuation in North America," JGR, 80, 4904-4916.
- Mueller, R. A. and J. R. Murphy (1971), "Seismic Characteristics of Underground Nuclear Detonations," BSSA, 61, 1693-1704.

- Oliver, J. (1962), "A Summary of Observed Surface Wave Dispersion," BSSA, 52, 81-86.
- Patton, H. (1980), "Crust and Upper Mantle Structure of the Eurasian Continent from the Phase Velocity and Q of Surface Waves," Reviews of Geophysics and Space Physics, 18, 605-625.
- Rodi, W. L., J. M. Savino, T. G. Barker, S. M. Day and T. C. Bache (1978), "Analysis of Explosion-Generated Surface Waves in Africa, Results from the Discrimination Experiment and Summary of Current Research," Systems, Science and Software Report SSS-R-78-3653, submitted to DARPA, April.
- Savino, J. M., C.B. Archambeau and J. F. Masso (1980), "VFM Discrimination Results from a Ten Station Network," Systems, Science and Software Technical Report submitted to VELA Seismological Center, VSC-TR-81-29 (SSS-R-80-4566), July.
- Singh (1982), "Anelasticity of the Crust and Upper Mantle Beneath the Eurasian Continent and the Nearby Regions from the Inversion of Love and Rayleigh Wave Attenuation Data," Geophys. J. R. Astr. Soc., 71, 761-774.
- Stevens, J. L. (1982), "A Model for Tectonic Strain Release from Explosions in Complex Prestress Fields Applied to Anomalous Seismic Waves from NTS and Eastern Kazakh Explosions," Systems, Science and Software Technical Report submitted to DARPA, VSC-TR-82-20 (SSS-R-82-5358), January.
- Stevens, J. L. and S. M. Day (1985), "The Physical Basis of m_b : M_s and Variable Frequency Magnitude Methods for Earthquake/Explosion Discrimination," JGR, 90, pp. 3009-3020.
- Stevens, J. L., W. L. Rodi, J. Wang, B. Shkoller, E. J. Halda, B. F. Mason and J. B. Minster (1982), "Surface Wave Analysis Package and Shagan River to SR0 Station Path Corrections," S-CUBED Topical Report submitted to VELA Seismological Center, VSC-TR-82-21 (SSS-R-82-5518), April.
- Sykes, L. R. and I. L. Cifuentes (1984), "Yields of Soviet Underground Nuclear Explosions from Seismic Surface Waves: Compliance with the Threshold Test Ban Treaty," Proc. Natl. Acad. Sci. USA, 81, pp. 1922-1925.
- Wang, J., J. L. Stevens, W. L. Rodi, J. B. Minster and B. F. Mason (1981), "Inversion of Surface Waves for Path Structure and Attenuation," Systems, Science and Software Topical Report, VSC-TR-82-13 (SSS-R-82-5232), submitted to VELA Seismological Center, November.